Convergent evolution on *RBA1* regulates *Candidozyma auris* host adaptation

Laura A. Doorley[1], Alyssa A. La Bella[2], Sarah J. Jones[1], Guolei Zhao[3], Mohammad Asadzadeh[4], Quanita J. Choudhury[1], Suhail Ahmad[4], Eiman Mokaddas[4,5], Inaam Al-Obaid[6], Wadha Alfouzan[4,7], Khalifa Al-Banwan[4,8], Teresa R. O'Meara[3] Felipe H. Santiago Tirado[2], Ana L. Flores Mireles[2], Jeffrey M. Rybak[1*]

[1] Department of Pharmacy and Pharmaceutical Sciences, St. Jude Children's Research Hospital, Memphis, TN 38105, USA.
[2] Department of Biological Sciences, University of Notre Dame, Notre Dame, IN 46556, USA
[3] Department of Microbiology and Immunology, University of Michigan, Ann Arbor, MI 48109, USA.
[4] Department of Microbiology, Faculty of Medicine, Kuwait University, Jabriya 46300, Kuwait.
[5] Department of Microbiology, Ibne-Sina Hospital, Shuwaikh, Kuwait
[6] Department of Microbiology, Al-Sabah Hospital, Shuwaikh, Kuwait
[7] Department of Microbiology, Farwaniya Hospital, Farwaniya, Kuwait
[8] Department of Microbiology, Amiri Hospital, Kuwait City, Kuwait

[*]Corresponding author: Jeffrey.Rybak@stjude.org

Jeffrey M. Rybak, PharmD, PhD
Assistant Member
Department of Pharmacy and Pharmaceutical Sciences
St. Jude Children's Research Hospital
262 Danny Thomas Place
Chili's Care Center, I5304, Mail Stop #313
Memphis TN, 38105

Office: 901.595.2368
Fax: 901.595.3125

ABSTRACT

Candidozyma auris is an emerging healthcare-associated fungal pathogen, increasingly isolated from clinical outbreaks, with a high propensity to colonize patients and the medical environment. Here, we leveraged *C. auris* isolates from multi-facility clinical outbreaks to identify genomic patho-adaptations promoting persistence and dissemination in the healthcare environment. Genomic and phylogenetic analyses revealed loss-of-function mutations in the uncharacterized *C. auris* transcription factor gene *RBA1* to have independently emerged multiple times within these outbreaks. We demonstrate loss of *RBA1* increases *C. auris* adhesion to plastic and human keratinocytes, enhances biofilm formation, and exacerbates fungal burden in a mouse model of catheter-associated urinary tract infection. Finally, we uncover mutations in *RBA1* have emerged during multiple *C. auris* outbreaks across the globe, and that *RBA1* mutant lineages are present among large ongoing clinical outbreaks. These results reveal loss-of-function mutations in *C. auris* *RBA1* as a novel and clinically relevant genetic determinant of enhanced outbreak characteristics.

52 **INTRODUCTION**

53 *Candidozyma auris* (formerly *Candida auris*) is an emerging pathogenic yeast first
54 identified in 2009 and later recognized by the World Health Organization as a critical threat to
55 global public health in 2022[1, 2]. Initially isolated from a limited number of individual patient
56 infections, *C. auris* was soon revealed as the cause of multiple nosocomial outbreaks of invasive
57 fungal infections across the globe[3]. Now, *C. auris* outbreaks have been reported from more than
58 50 countries, representing thousands of documented infections annually, including 4,514 cases
59 in 2023 in the United States alone[4, 5, 6]. *C. auris* is distinguished from other fungal pathogens as it
60 is not known to be ubiquitous within common natural environmental reservoirs nor is it a member
61 of the normal human microbiota[7]. Instead, *C. auris* infections are healthcare-associated and
62 typically occur following a lateral transmission to vulnerable patients within hospital settings[8].
63 Multiple studies have demonstrated that once introduced into the medical environment, *C. auris*
64 rapidly spreads among both patients and medical surfaces, acting as an invasive species in these
65 healthcare settings. As a result, clinical *C. auris* infections routinely occur in series or as clustered
66 clinical outbreaks, sometimes spanning multiple facilities or institutions within an affected
67 healthcare network[9, 10].

68 As with other healthcare-associated and multi-drug-resistant pathogens, the
69 characterization and tracking of emergent microbial lineages with traits impacting clinical
70 outcomes is paramount to infection prevention and treatment. Prior study of *C. auris* evolution
71 during infection and exposure to clinically relevant stressors has largely focused on the
72 emergence of antifungal resistance[11, 12, 13, 14]. We and others have shown, through both *in vitro*
73 evolution experiments and by studying sets of isogenic clinical isolates, that *C. auris* is capable
74 of rapidly adapting to antifungal-induced stress and that multiple independent drug-resistant
75 lineages can emerge after only a single antifungal exposure[11, 12, 13, 14]. However, investigations of
76 patho-adaptation in the clinical setting or during outbreaks of infections remains unexplored.

77 In this work, we leveraged a collection of *C. auris* clinical isolates from multi-institutional
78 outbreaks of infection to identify novel genetic markers and link them to traits driving host
79 adaptation and outbreak potential in clinical settings. We identified multiple independent lineages
80 of *C. auris* harboring distinct mutations in a previously uncharacterized fungal transcription factor,
81 here named, Repressor of Biofilm and Adhesion 1 (*RBA1*). Genetic and transcriptomic
82 interrogation revealed loss of *RBA1* to result in enhanced biofilm formation, increased adhesion
83 to multiple surfaces including human keratinocytes, and significantly elevated expression of
84 *C. auris* adhesins and virulence factors. Moreover, loss of *RBA1* was found to significantly
85 increase fungal burden in a mouse model of catheter-associated urinary tract infection (CAUTI),
86 an infection characteristically involving biofilms in urine where *C. auris* is often isolated[15]. Finally,
87 analysis of publicly available whole genome sequencing data revealed numerous distinct *RBA1*
88 mutations present in hundreds of clinical isolates, demonstrating consistent and convergent loss-
89 of-function mutations from isolates from well-documented and ongoing clinical outbreaks of
90 *C. auris* infections across the globe. Collectively these findings demonstrate *RBA1* encodes a
91 repressor of *C. auris* biofilm and adhesion and implicate mutations in *RBA1* as clinically relevant
92 adaptations promoting *C. auris* survival during healthcare-associated outbreaks of infection.
93
94 **RESULTS**
95 **Clinical emergence of multiple *C. auris* outbreak lineages carrying *RBA1* mutations.**
96 Whole genome sequencing (WGS) analysis revealed all *C. auris* isolates belonged to
97 Clade I, one of three major genetic clades previously linked to healthcare-associated outbreaks[16].
98 This included 34 and 36 isolates from the previously described subclades Ib and Ic, respectively[17].
99 A total of 155,135 SNPs were identified among the 70 included isolates as compared to the Clade
100 I reference genome (B8441v3), with 46,231 predicted to impact coding regions. As anticipated
101 from characteristically fluconazole-resistant Clade I isolates, all isolates were found to harbor one
102 or more mutations in the genes *ERG11*, *TAC1B*, and/or *MRR1*, which we and others have

103 previously shown to directly contribute to fluconazole resistance[14, 18, 19, 20]. Additionally, 16 isolates
104 were found to possess mutations known to contribute to echinocandin resistance (altering *FKS1*)
105 and 4 isolates possessed mutations in genes associated with amphotericin B (AmB) resistance
106 (*ERG3*, 1 isolate; *ERG6*, 3 isolates)[12, 21, 22].

107 Phylogenetic analysis revealed the population structure of this collection to consist of 69
108 isolates grouping into three major clusters, with 35, 24, and 10 isolates grouping into clusters A,
109 B, and C, respectively (**Fig. 1**). A single isolate (SKU043) did not group into a larger cluster and
110 was more distantly related. Within clusters, isolates were found to be largely clonal, with an
111 average of 5.3 to 12.6 coding region SNPs separating each isolate (**Fig. S1**), while SKU043
112 differed from all other isolates by 43 to 113 coding region SNPs. Clusters A and C each contained
113 isolates originating from multiple healthcare facilities within Kuwait, while cluster B originated
114 entirely from a single tertiary care hospital. Notably, multiple instances were identified where
115 isolates from different patients and even different hospitals were found to be more genetically
116 similar than serial isolates originating from the same patient case, as might be expected in the
117 setting of a clinical outbreak.

118 To investigate potential patho-adaptations occurring during outbreaks of *C. auris*
119 infections, we further evaluated the WGS data to identify genes where mutations were acquired
120 on multiple occasions and/or mutations emerged and persisted among the outbreak population.
121 Intriguingly, this revealed 19 isolates harboring mutations in a previously uncharacterized *C. auris*
122 gene B9J08_03209 (identified as B9J08_002136 in B8441v2 and hereafter named *RBA1*), which
123 is predicted to encode a fungal-specific zinc-cluster transcription factor (ZCF). Although initially
124 identified as an ortholog of *WOR2* in *C. albicans,* the proteins are not syntenic, with only 22%
125 sequence identity, primarily located in the DNA-binding domain. The 19 isolates with mutations in
126 *RBA1* included representatives from all three major phylogenetic clusters, including all 10 isolates
127 in cluster C, as well as the non-clustered isolate SKU043. Four different mutations in *RBA1* were
128 identified, all considered likely loss-of-function mutations, with three encoding an early stop codon

129 (upstream of the predicted DNA-binding domain) and one altering a highly conserved cysteine
130 residue in the $Zn(II)_2Cys_6$ DNA-binding motif. The early stop codon mutation, *RBA1*^{E47*}, was found
131 to have emerged and persisted among two intensive care unit (ICU) patients, these cases and
132 the associated isolates were further evaluated to identify the potential clinical impact of *RBA1*
133 mutations.
134
135 **Loss of *RBA1* enhances *C. auris* biofilm formation.**
136 A subset of isolates from patient cases 51 and 53 have been previously characterized with
137 consideration to antifungal susceptibility while investigating the emergence of echinocandin and
138 amphotericin B resistance-conferring mutations, respectively[12, 23, 24]. In brief, both were adult
139 patients with complex medical histories including hematologic malignancies admitted to the ICU
140 of a tertiary care center and received multiple courses of the antifungals liposomal amphotericin
141 B (AmB) and caspofungin (CSF). Over the course of approximately eight months, a total of 14 *C.*
142 *auris* isolates were cultured from the respiratory tract, urinary tract, and blood of patients 51 and
143 53 (**Fig. 2a**). Notably, while the earliest isolate in these cases, SKU013, harbored a wildtype *RBA1*
144 allele (*RBA1*^{WT}), an early stop codon encoding mutation in *RBA1* (*RBA1*^{E47*}) emerged in an isolate
145 obtained from culturing the urinary catheter (SKU018). This mutation was subsequently found in
146 all but one *C. auris* isolate cultured from patient 53. Further details of these cases can be found
147 in **Supplemental Data**
148 Of the 14 isolates cultured from patient 51 and patient 53, 13 were found to be closely
149 related (separated by 2 to 8 SNPs within coding regions, **Fig. S1**) and grouped into cluster B.
150 While *RBA1* mutant isolates were observed to exhibit increased biofilm formation under standard
151 laboratory conditions, there was no association between antifungal susceptibility and *RBA1*
152 genotype, (**Fig. 2b, c**). As the earliest isolate where the *RBA1*^{E47*} mutation was present (SKU018)
153 was cultured from the urinary tract of patient 51, and multiple subsequent isolates with this
154 mutation were isolated from the urinary tract of patient 53, we used our fibrinogen-urine biofilm

155 model [25] that utilizes serum-supplemented urine and fibrinogen-coated surfaces to evaluate
156 biofilm formation in conditions mimicking the bladder during CAUTI. In this model, isolates
157 carrying the *RBA1*^{E47*} mutation exhibited enhanced biofilm formation as compared to the earliest
158 isolate SKU013 (approximately 2 to 6-fold higher), while biofilm formation was relatively
159 unchanged among closely related *RBA1*^{WT} isolates (**Fig. 2d**). To evaluate if other clinically
160 emergent predicted loss-of-function mutations in *RBA1* had a similar effect on biofilm formation,
161 we also compared the biofilm formation of isolates harboring the *RBA1*^{Q174*} (SKU055), *RBA1*^{Q225*}
162 (SKU043), and *RBA1*^{C303S} (SKU056) mutations to their closest available genetic relatives
163 (SKU021, SKU034, and SKU037, respectively) using the same model. In each case, biofilm
164 formation was observed to be significantly higher in the isolates harboring mutations in *RBA1*
165 (**Fig. 2e**), further bolstering the connection between loss of *RBA1* and biofilm formation.

166 From these observations, we hypothesized that loss-of-function mutations in *RBA1* are a
167 genetic determinant of enhanced *C. auris* biofilm formation. To test this hypothesis, we next
168 generated the *RBA1*-knockout (*Δrba1*) and *RBA1*-revertant (*Δrba1*::*RBA1*$^{+}$) control strains in the
169 SKU013 clinical isolate background and evaluated biofilm formation. In the fibrinogen-urine
170 model, *Δrba1* strains were found to exhibit significantly increased biofilm formation (3.9 to 4.8-fold
171 greater than SKU013; $p<0.0001$). This enhancement of biofilm formation resembled the isogenic
172 clinical isolate SKU018 which carries the *RBA1*^{E47*} mutation (3.3-fold greater than SKU013;
173 $p<0.0001$) (**Fig. 3a**). Importantly, restoration of the *RBA1* gene in *Δrba1*::*RBA1*$^{+}$ control strains
174 returned biofilm formation to levels comparable to SKU013.

175 We further investigated the impact of *RBA1* using a plasma-RPMI biofilm model that
176 utilized serum-supplemented RPMI culture media and human plasma-coated surfaces to evaluate
177 biofilm production that could apply more generally to clinical settings. Once again, *Δrba1* strains
178 were found to produce more robust biofilms (6.2 to 6.8-fold greater than SKU013; $p<0.0001$),
179 while *Δrba1*::*RBA1*$^{+}$ control strains closely matched the biofilm formation of SKU013 (**Fig. 3b**).
180 Examination of the plasma-RPMI biofilms using scanning electron microscopy, showed scattered

181 patches of biofilm predominantly consisting of one to two layers of cells for both SKU013 and
182 *Δrba1*::*RBA1*$^{+}$ (**Fig. 3c**). By comparison, *Δrba1* strains formed more confluent biofilms of variable
183 but generally greater thickness with greater production of extracellular matrix. (**Fig. 3d**).
184
185 **Loss of *RBA1* increases expression of *C. auris* adhesins and virulence factors.**
186 As *RBA1* is predicted to encode a transcription factor and our earlier experiments had
187 shown loss of *RBA1* significantly enhances biofilm formation, we next evaluated the impact of
188 *RBA1* on the *C. auris* transcriptome during both planktonic and biofilm growth conditions using
189 our *Δrba1* strain and the parental *RBA1*^{WT} isolate SKU013. When cells were grown in RPMI tissue
190 culture media under planktonic conditions, transcriptional profiling revealed loss of *RBA1* to have
191 a modest impact, and only 55 of 5,594 *C. auris* genes (0.98%) were differentially expressed (≥|1.5|
192 fold-change and false discovery rate [FDR] ≤0.05) (**Fig. 4a**). Of these, 42 genes were upregulated
193 in the absence of *RBA1*, and these genes were enriched for those involved in biofilm formation
194 (p= 1.60e-07) and cell aggregation (p= 2.18e-07), and no enrichment for biological processes was
195 found among the 13 down-regulated genes. By comparison, when cells were harvested from
196 actively growing biofilms, 701 of 5,594 genes (12.53%) were observed to be differentially
197 expressed, including 250 and 451 genes which were up- and down-regulated in the *Δrba1* strain,
198 respectively (**Fig. 4b**). Up-regulated genes were enriched for those involved in transmembrane
199 transport (p= 0.01351), regulation of RNA biosynthetic process (p=0.02583), cell aggregation
200 (p=0.05187), and regulation of primary metabolic process (p=0.07722), while down regulated
201 genes were enriched for 18 different biological processes including protein biosynthetic process
202 (p= 2.35e-28), macromolecule biosynthetic process (p= 4.05e-10), premeiotic DNA replication (p=
203 0.00273), and steroid biosynthetic process (p= 0.02579). Thirty-two *C. auris* genes were up-
204 regulated in the absence of *RBA1* under both growth conditions, and these genes were enriched
205 for those involved in biofilm formation and cell aggregation (**Fig. 4c**). Notably, this included four

206 *C. auris* adhesins (*ALS4112/ALS5, IFF4*, *IFF4109*, and *SCF1*), three of which we have previously
207 shown to impact virulence in a mouse model of invasive candidiasis[26, 27].
208 As many genes in the *C. auris* genome remain uncharacterized and/or currently have
209 incomplete annotations, we further evaluated differential expression among *C. auris* genes with
210 homology to those associated with adhesion, biofilm formation, and cell wall architecture in the
211 model pathogenic yeast *Candida albicans.* This revealed additional *C. auris*-specific adhesins,
212 cell wall-associated proteins, GPI-anchored proteins, and aspartic-type endopeptidases
213 exhibiting differential expression under biofilm conditions in the absence of *RBA1* (**Fig. 4d**).
214 Notably, four of the differentially expressed genes associated with the fungal cell wall,
215 B9J08_002109, B9J08_003350, *PHR1*, and *XOG1*, are the predicted orthologs of *C. albicans* cell
216 wall proteins known to be involved in cell wall remodeling, cell wall masking from immune
217 detection, and response to host immune cells[28, 29, 30].
218 As *RBA1* appears to repress biofilm formation in *C. auris,* we also examined the
219 expression of *C. auris* orthologs of genes known to regulate biofilm formation in the model
220 pathogenic yeast, *C. albicans* (**Fig. 4d**). *UME6* and B9J08_002529 (ortholog of *C. albicans*
221 *BRG1*), exhibited significantly increased expression in the *Δrba1* strain under planktonic
222 conditions. In *C. albicans,* these genes are known to be important positive regulators of hyphal
223 growth and biofilm formation. Further, *UME6* has previously been shown to impact *C. auris* biofilm
224 formation when overexpressed and artificially hyper-activated through HA-tagging of the putative
225 transcription factor activation domain[31]. Under biofilm conditions, 14 genes orthologous to those
226 known to regulate biofilm formation in *C. albicans* were up-regulated, notably again including the
227 *C. auris* orthologs of *BRG1.* These findings demonstrate that *RBA1* significantly impacts
228 regulation of *C. auris* gene expression during biofilm formation and suggest that *RBA1* may play
229 a central regulatory role in this clinically impactful process.
230
231 **Loss of *RBA1* enhances *C. auris* adhesion to plastics and human keratinocytes**

232 A key clinical characteristic of *C. auris* is its ability to adhere to and persist on a variety of
233 surfaces in the nosocomial environment, including medical equipment and patient skin. As our
234 transcriptional profiling revealed loss of *RBA1* enhanced the expression of an assortment of
235 *C. auris* adhesin-encoding genes, we hypothesized that loss of *RBA1* would enhance *C. auris*
236 adhesion to multiple substrates. To test this, we first evaluated the adherence of our *Δrba1* and
237 *Δrba1*::*RBA1*$^{+}$ strains, as well as the isogenic clinical isolates SKU013 and SKU018, to
238 polystyrene plastic under a variety of conditions. In RPMI media, SKU018 and the *Δrba1* strains
239 exhibited greater adhesion than SKU013 to both polystyrene and tissue culture-treated
240 polystyrene (**Fig. 5a, b**). This difference was magnified when the polystyrene well plates were
241 pre-treated with human plasma, with or without the addition of 10% human serum to the media
242 (**Fig. 5c, d**). By contrast, *Δrba1*::*RBA1*$^{+}$ control strains phenocopied the parental SKU013 under
243 all conditions.
244 Next, we evaluated whether loss of *RBA1* promotes adhesion of *C. auris* to human
245 keratinocytes. *Δrba1* strains were observed to exhibit enhanced adherence to a confluent culture
246 of human N/TERT keratinocytes, while neither *Δrba1*::*RBA1*$^{+}$ controls strains nor SKU018 differed
247 from the SKU013 control (**Fig. 5e** (top)**, f**). Outbreak isolates harboring the *RBA1*^{Q174*} (SKU055),
248 *RBA1*^{Q225*} (SKU043), and *RBA1*^{C303S} (SKU056) mutations were similarly found to exhibit
249 enhanced adhesion to keratinocytes as compared to their closest available genetic relatives (**Fig.
250 5e** (bot)**, g**) further supporting the connection between loss of *RBA1* and enhanced adherence to
251 human keratinocytes. Taken together, these results confirm that loss of *RBA1* significantly
252 enhances *C. auris* adhesion characteristics under a variety of conditions.
253
254 **Loss of *RBA1* increases fungal burden during catheter-associated urinary tract infections.**
255 As loss of *RBA1* increased *C. auris* adhesion, biofilm formation, and the expression of the
256 previously characterized virulence factors *SCF1*, *IFF4109*, and *ALS4112/ALS5*, we next sought

257 to evaluate the impact of *RBA1* on *C. auris* biofilm-related infection *in vivo.* To accomplish this,
258 we utilized our mouse model of CAUTI [25, 32], where immunocompetent mice were catheterized
259 and the bladder of each mouse was challenged with *C. auris* transurethrally 24 hours prior to
260 sacrifice for evaluation of fungal burden and systemic dissemination of infection. Importantly, this
261 mimics a clinical scenario where *C. auris* is often cultured from patients with urinary catheters and
262 is relevant to multiple patient populations at increased risk of *C. auris* colonization and infection.
263 In this model, the *Δrba1* strain was found to exhibit a 6.8-fold increase in bladder tissue fungal
264 burden (p= 0.0435) by 24 hours post-infection, as compared to SKU013 (**Fig. 5h**). Moreover, a
265 trend toward increased dissemination of the *Δrba1* strain to kidney and spleen tissues was also
266 observed, and one mouse infected with the *Δrba1* strain was found to have detectable fungal
267 burden in cardiac tissue. These findings suggest that loss of *RBA1* may also enhance virulence
268 of *C. auris* during clinical infections such as CAUTI.
269

270 **Mutations in *RBA1* have emerged during numerous *C. auris* clinical outbreaks**

271 We next hypothesized that *RBA1* mutations have also likely occurred during other *C. auris*
272 outbreaks as well. To test this, we leveraged publicly available *C. auris* WGS data collected for
273 infection control and outbreak tracking to identify mutations in the *RBA1* gene. Ninety-four
274 mutations in *RBA1* were identified, and 310 of 2,181 evaluable isolates were found to carry one
275 or more of 58 identified non-synonymous or nonsense *RBA1* mutations, including *C. auris* isolates
276 representing genetic clades I, II, and IV. The majority of the identified non-synonymous/nonsense
277 mutations are considered as likely loss-of-function mutations (40; 61.5%) (**Fig. 6a**), similar to the
278 mutations we initially identified from the Kuwait outbreak collection. Evaluating meta data and
279 publications associated with identified isolates revealed 10 non-synonymous *RBA1* mutations
280 originating from documented outbreaks of *C. auris* infection on four continents and were caused
281 by isolates representing both genetic clades I and IV (**Fig. 6b**) [10, 16, 33, 34, 35, 36]. Notably, this included
282 two instances where *RBA1* mutations arose during Indian outbreaks[37] initially reported in 2013,

283 as well as two instances of *RBA1* mutations occurring during ongoing outbreaks in the United
284 States[34, 38]. These findings clearly demonstrate convergent mutations in *RBA1* across multiple of
285 *C. auris* outbreaks and further suggest that these mutations confer a competitive advantage to *C.*
286 *auris* in the healthcare environment.
287
288 **DISCUSSION**
289 *C. auris* is frequently associated with clinical outbreaks of infection and multi-drug
290 resistance thus posing a challenge to clinicians reminiscent of the healthcare-associated bacterial
291 pathogens, *Acinetobacter baumannii* and *Enterococcus faecium*, [3, 8]. Unlike other agents of
292 invasive candidiasis, *C. auris* is not considered as part of the human normal flora and is not known
293 to be widely distributed in environmental reservoirs. Instead, *C. auris* infections are currently
294 thought to be acquired predominantly through dissemination of recently emergent drug-resistant,
295 and possibly infection-adapted, lineages within medical environments, leading to the infection of
296 vulnerable patient populations[3, 16]. Thus, as with other healthcare-associated pathogens, the
297 identification of *C. auris* evolution during clinical outbreaks and characterization of traits promoting
298 the persistence among human patients is essential to both preventing infections and mitigating
299 prolonged outbreaks of infection.
300 Here, we analyzed samples from outbreaks in Kuwait to identify genomic and
301 microbiological elements which may promote transmission and persistence of *C. auris* in clinical
302 settings. Rather than distinct clustering of serial isolates from individual patient cases,
303 phylogenetic analysis identified isolate clusters originating from multiple patients indicating
304 multiple instances of pathogen lateral transmission consistent with clinical dissemination.
305 Interestingly, while numerous cases of isolates acquiring mutations associated with echinocandin
306 and AmB resistance were identified, persistence and spread of these multi-drug-resistant lineages
307 was not observed in this study. Conversely, among both phylogenetic clusters B and C, closely
308 related isolates harboring acquired *RBA1* mutations were cultured from multiple patients over

309 periods of time spanning many months. While there was no association between clinical
310 antifungal susceptibility and *RBA1* genotype, *C. auris* isolates carrying clinically acquired loss-of-
311 function mutations in *RBA1* were observed to exhibit enhanced biofilm formation as compared to
312 those with wildtype *RBA1* sequences.

313 Biofilms are critically important to human public health as they promote microbial survival
314 in a variety of environments, demonstrating increased resilience to disinfectants and
315 antimicrobials, and contribute to pathogen dissemination and the establishment of new infections.
316 In fact, the majority of human infections involve biofilms either within human tissues or on the
317 surface of in-dwelling medical devices such as catheters or prosthetic implants [39]. As numerous
318 clinical isolates from the studied clinical outbreaks in Kuwait were isolated from the urine of
319 catheterized patients or the respiratory secretions of patients with endotracheal tubes, we
320 hypothesized that the identified loss-of-function mutations in *C. auris RBA1* represented a
321 clinically emergent adaptation promoting pathogen success in the medical environment through
322 enhanced biofilm formation. Genetic interrogation of the impact of *C. auris RBA1* definitively
323 demonstrated loss of this gene enhanced biofilm formation when evaluated using *in vitro* models
324 mimicking clinically relevant conditions including those specific to CAUTI. This enhancement of
325 biofilm formation may represent a selective pressure which promoted the emergence and
326 persistence of *RBA1* mutant lineages during the studied clinical outbreaks.

327 Subsequent transcriptional profiling revealed a narrow role in *C. auris* cells growing under
328 planktonic conditions, and a much wider influence on gene expression when cells were grown in
329 biofilms. Under both conditions, however, *Δrba1* strains exhibited increased expression of a
330 multitude of cell surface adhesins, including multiple genes we have previously shown to
331 significantly impact *C. auris* virulence during infection. The two previously characterized *C. auris*-
332 specific adhesins, *SCF1* and *ALS4112/ALS5,* were substantially elevated in the *Δrba1* strain
333 grown in planktonic conditions, with both genes exceeding a 7-$\log_2$-fold increase over the SKU013
334 parental control. As these adhesins are known to be critical to the ability of *C. auris* to adhere to

335 a variety of substrates including human skin[26, 27], this suggested that *RBA1* may impact the
336 propensity of *C. auris* to both colonize patients and establish new biofilms. Further investigation
337 of gene expression in biofilms demonstrated a wide variety of genes predicted to encode *C. auris*
338 cell surface proteins, cell wall constituents, secreted enzymes, and transcriptional regulators were
339 differentially expressed in the *Δrba1* strain. Intriguingly, this also included the *C. auris* orthologs
340 of *C. albicans ENG1* and *YWP1*, two secreted beta-glucanases which are known to play critical
341 roles in cell wall beta-glucan masking[28, 29, 30]. This finding, combined with the altered expression
342 of a multitude of GPI-anchored cell surface proteins and the differences in extracellular matrix
343 production observed by scanning electron microscopy, suggests that the loss of *RBA1* may also
344 facilitate evasion of *C. auris* detection from host defenses during infection.

345 We next examined whether loss of *RBA1* and subsequent increased expression of *SCF1*
346 and *ALS4112/ALS5* would impact the ability of *C. auris* to adhere to surfaces where *SCF1* and
347 *ALS4112/ALS5* play a significant role[26, 27]. Strains lacking *RBA1* were found to exhibit enhanced
348 adhesion to human keratinocytes as well as polystyrene surfaces both with and without human
349 plasma coatings, which mimics the deposition of host factors such as fibrinogen on medical device
350 surfaces. Moreover, evaluation of three *C. auris* clinical isolates from the Kuwait outbreaks
351 harboring three additional loss-of-function mutations, as compared to their respective closest
352 available genetic relative with a *RBA1*^{WT} allele, again demonstrated loss of *RBA1* to increase
353 adhesion of *C. auris* to human keratinocyte. This finding is of substantial clinical relevance, as it
354 supports that loss of *RBA1* can promote the dissemination of *C. auris* and colonization of patients
355 during a clinical outbreak. Further, patients colonized with *C. auris* strains harboring *RBA1* loss-
356 of-function mutations may pose a greater risk of transmission within the hospital environment.

357 We also examined the impact of *RBA1 in vivo* using a murine CAUTI model which
358 replicates a biofilm-related infection of a site where *C. auris* is commonly isolated. Contrary to
359 other commonly utilized models of pathogenic yeast infection, this model uses mice that have not
360 been immunosuppressed. Instead, immunocompetent mice are made vulnerable to *C. auris*

361 infection through the implantation of a silicone catheter, similar to urinary catheters commonly
362 used among human patients. In this model, the *Δrba1* strain was found to develop a significantly
363 greater fungal burden in the mouse bladder, and a trend towards greater dissemination of the
364 *Δrba1* strain from the urinary tract to other tissues including the heart was observed. These
365 findings further suggest loss of *RBA1* is advantageous during *C. auris* clinical infection. This is
366 clinically significant as CAUTIs often lead to urosepsis with a ~30% 7-day mortality rate [15, 40].
367 Since the urinary tract is a source of ~25% of the all the sepsis cases, patients infected with
368 *C. auris* strains harboring *RBA1* mutation may be predisposed to severe clinical complication.
369 Finally, leveraging the growing body of publicly available WGS data generated through
370 ongoing *C. auris* infection control and prevention efforts, we were able to investigate whether
371 mutations in *RBA1* have emerged during other clinical outbreaks. This approach uncovered
372 dozens of distinct *RBA1* mutations, impacting hundreds of clinical isolates and more than 10% of
373 evaluable samples. *RBA1* mutations were identified among isolates representing three of the
374 major genetic subgroups of *C. auris,* but were notably absent among isolates from clade III*,*
375 suggesting either clade-specific impacts of *RBA1* mutations or a potential bias within samples
376 currently available in the public data set. Like the four *RBA1* mutations identified from the Kuwait
377 outbreaks, the mutations identified from the global collection were predominantly predicted loss-
378 of-function mutations such as those encoding early stop codons, frameshift mutations, or altering
379 highly conserved residues in the ZCF DNA-binding domain. Identified isolates with *RBA1*
380 mutations were found to date back to some of the earliest documented clinical outbreaks of
381 *C. auris*, including those in India, England, and Columbia. Additionally, isolates from outbreak
382 lineages actively disseminating in the United States were also found to harbor *RBA1* mutations.
383 Taken together, these findings clearly demonstrate that mutations in *RBA1* have emerged
384 repeatedly during clinical outbreaks of *C. auris* infection and strongly support the notion that the
385 enhancement in adhesion and biofilm formation conferred by these mutations provided a
386 competitive advantage within the medical environment in numerous previous outbreaks.

387 In conclusion, these results call attention to the capacity of *C. auris* to evolve and enhance
388 traits beyond drug resistance during outbreaks of infection by highlighting the unique nature of
389 *C. auris* among other fungal pathogens and identifying mutations in *RBA1* as a potential indicator
390 of outbreak-adapted lineages. As traits conferred by *RBA1* mutations are advantageous to
391 *C. auris* spread and persistence, and as we have identified numerous instances where these
392 mutations have arisen during global outbreaks of infection, the identification and tracking of
393 lineages carrying *RBA1* mutations may be merited as part of infection prevention efforts.
394

395 **MATERIALS AND METHODS**

396 **Ethics Statement**

397 *C. auris* isolates were cultured from various clinical specimens of hospitalized patients in
398 Kuwait. The need for informed consent was waived by the Health Sciences Center Ethics
399 Committee (Approval letter Ref: VDR/EC/3724 dated January 31, 2021) as the clinical specimens
400 were collected as part of routine diagnostic work-up for the isolation of bacterial/fungal pathogens
401 for suspected infections. The results are reported here on deidentified samples without revealing
402 patient identity. All animal care was consistent with the Guide for the Care and Use of Laboratory
403 Animals from the National Research Council. The University of Notre Dame Institutional Animal
404 Care and Use Committee approved all mouse infections and procedures as part of protocol
405 number 25-01-9009. For urine collection, all donors signed an informed consent form, and
406 protocols were approved by the Institutional Review Board of the University of Notre Dame under
407 study #19-04-5273.

408

409 ***C. auris* Isolates**

410 Seventy *C. auris* isolates from previously described multi-institution outbreaks of *C. auris*
411 infections in Kuwait, were obtained by the Mycology Reference Laboratory Department of
412 Microbiology, Kuwait University, Kuwait [41]. All isolates (including names used in publication of
413 their original description) and strains used in this study are listed in **Table S1**. All *C. auris* strains
414 were stored in 40% glycerol stocks at -80°C and cultured at 35°C in liquid YPD (1% yeast extract,
415 2% peptone, 2% glucose) media before plating on Sabouraud dextrose (SD) agar (BD Difco)
416 media to ensure standardized growth for phenotypic testing.

417

418 **Plasmid and strain construction**

419 EPIC-mediated gene editing was used to generate *RBA1* (B8441v3: B9J08_03209)
420 modifications in *C. auris* clinical isolate SKU013 (also known as Kw1432/17). Duplexed guide

421 oligos (Integrated DNA Technologies) (**Table S2**) targeting disruption or reversion of
422 B9J08_03209 were added to the pJMR19 vector using restriction enzyme cloning[22]. Plasmids
423 were maintained in *E. coli* DH5α cells cultured in Luria-Bertani broth supplemented with 5mg/L
424 ampicillin and isolated using QIAprep® Spin Minipreps (Qiagen). Repair templates for *RBA1*-
425 disruption and reversion were amplified from a gBlock sequence (Integrated DNA Technologies)
426 and SKU013 gDNA, respectively, via PCR and purified with QIAquick PCR Purification Kit
427 (Qiagen). All oligos, plasmids, and gBlocks used in this study are listed in **Table S2.** *C. auris*
428 Lithium acetate transformations were then performed as previously described [22] with positive
429 selection on 200µg/mL nourseothricin-supplemented YPD agar. *RBA1* editing was confirmed by
430 both Sanger sequencing at the Hartwell Center at St. Jude Children's Research Hospital (SJCRH)
431 and with long read nanopore sequencing by Plasmidsaurus.
432
433 **Whole genome sequencing**
434 Genomic DNA (gDNA) was extracted from 1mL of overnight liquid YPD cultures using
435 MasterPure™ Yeast DNA Purification kits (Biosearch Technologies) according to manufacturer
436 instructions. Sample libraries were prepared from gDNA by the Hartwell Center (SJCRH) using
437 KAPA HyperPrep (Roche) and sequencing targeting 100x coverage for paired 150bp reads was
438 performed via Illumina NovaSeq. Paired-reads FASTQ files were analyzed using CLC genomics
439 workbench v24.0 (QIAGEN) software. Low quality reads were trimmed with Trim Reads v2.8 and
440 subsequently mapped to the B8441v3 genome (GCA002759435.3) according to CLC-workbench
441 recommendations for match scores, mismatch, insertion, and deletion costs. Local Realignment
442 v2.6 was used to refine unaligned ends and mutations were identified within annotated coding
443 sequences via Fixed Ploidy Variant Detection v2.6 with ploidy=1.
444 Phylogenetic analysis was initiated with Create SNP Tree v1.9 using the Maximum
445 Likelihood Phylogeny v1.4 algorithm. The resulting SNP phylogenetic tree was visualized from
446 Neighbor Joining construction methods specifying Jukes Cantor nucleotide substitution modeling

447 with estimated topology and bootstrapping for 100 replicates. Sequences were deposited in
448 National Center for Biotechnology Information Sequence Read Archive.
449
450 **Biofilm Production Assays**
451 To assess biofilm production in the presence of human plasma, 96-well flat-bottomed
452 plates (VWR, 10861-562) were coated with 100 μL pooled human plasma (Innovative Research
453 Inc, IPLAWBNAC50ML) diluted 1:5 in carbonate-bicarbonate buffer (Sigma C3041-50CAP) and
454 incubated overnight at 4°C. Colonies from overnight SD agar plates were used to generate
455 standardized OD_{600} = 0.5 cell suspensions[42] in RPMI-Biofilm media, consisting of RPMI medium
456 1640 (Gibco) + 3-(4-Morpholino)propane sulfonic acid (MOPS, Fisher Bioreagent) + 2% dextrose,
457 buffered to pH 7 and supplemented with 10% heat-inactivated/male AB human serum (HuS,
458 Sigma-Aldrich). Plasma coatings were gently removed the plates and 200 μL of the cell
459 suspensions were added to the wells and plates were sealed with a breathable (EASYSEAL)
460 membrane. After 90-minutes at 37°C, 250 RPM, plates were gently washed sterile PBS to remove
461 non-adhered cells. Fresh 200 μL of RPMI-Biofilm media was then added back to each well and
462 plates were incubated for 24 hrs at 37°C, 250 RPM. For quantification of biofilm production,
463 supernatants were removed and wells were gently washed twice with PBS. Biofilms were stained
464 with 0.4% crystal violet as previously described[42]. Crystal violet absorbance measured at 595nm
465 on an Agilent BioTek Synergy H1 Microplate Reader. Average media only negative controls were
466 subtracted from the sample reads and values were normalized to SKU013.
467 To replicate biofilm growth replicating the urinary tract environment, 96-well flat-bottomed
468 plates (VWR, 10861-562) were coated with 100 µl of Fg (450 µg/ml) and incubated overnight at
469 4°C.[25] The various strains were grown overnight, shaking in YPD, and the inoculum was
470 normalized to ~1 × 10^6 CFUs/ml. Cultures were then diluted (1:100) into human urine
471 supplemented with 10% heat inactivated human serum and incubated in the wells of the 96-well

472 plate at 37°C for 48 hours. Human urine from at least two healthy female donors between the
473 ages of 20 to 35 were collected and pooled. Donors did not have a history of kidney disease,
474 diabetes, or recent antibiotic treatment. Urine was sterilized with a 0.22-µm filter (VWR 29186-
475 212), pH was normalized to 6.0 to 6.5, and urine was used immediately for the assays. Following
476 biofilm formation, supernatants were removed, and plates were incubated in 200 µl of 0.5% crystal
477 violet for 15 min. Crystal violet stain was removed, and the plate was washed with water to remove
478 the remaining stain. Plates were dried and then incubated with 200 µl of 33% acetic acid for 15
479 min. In another plate, 100 µL of the acetic acid solution was transferred, and absorbance values
480 were measured via a plate spectrophotometer at 595 nm (Molecular Devices SpectraMax ABS).
481 Values were then normalized to SKU013.
482
483 **RNA Extraction**
484 Normalized cell suspensions (OD_{600} = 0.1) from SD replicate platings were diluted ~1:50
485 in 10 mL RPMI-Growth media, prepared from RPMI medium 1640 (Gibco) + MOPS (Fisher
486 Bioreagent) buffered to pH 7 and grown overnight at 35°C, 220 RPM to an OD_{600} = 2.0 ± 0.3.
487 Concentrated cultures were diluted in >20mL RPMI-Growth media to an OD_{600} = 0.2 then split
488 into two 10mL aliquots for direct comparison of planktonic growth and biofilm development.
489 Planktonic cells were grown over 4 hours in 50mL conical at 35°C, 220RPM and pelleted at 4000
490 RPM. For biofilm development cells were transferred to T75 flask pre-coated with 20% human
491 plasma in carbonate-bicarbonate buffer prepared as described above. Following 2 hr incubation
492 at 37°C, non-adhered cells were gently removed and fresh 10mL RPMI-Growth media was added
493 for an additional 4 hr incubation at 37°C. Biofilms were gently washed once with PBS and biofilms
494 were then removed by scraping in the presence of 10mL sterile PBS and pipette transfer to a
495 50mL conical tube for centrifuge pelleting. All pellets were flash frozen in liquid nitrogen and stored

496 at -80°C. RNA was isolated using the Invitrogen RiboPure™ Yeast kit (ThermoFisher Scientific™,
497 USA) per manufacturer's instructions.
498
499 **RNA Sequencing**
500 The Hartwell Center (SJCRH) prepared the RNA libraries using Illumina chemistries per
501 manufacturer's instructions and sequenced the RNA on an Illumina NextSeq (Illumina Inc., USA)
502 using the total stranded RNA-Seq application for paired end runs targeting 150bp reads.
503 Sequenced reads were analyzed with CLC Genomics Workbench version 24.0.1 (QIAGEN).
504 Imported reads were trimmed using default settings for failed reads and adaptor sequences and
505 then subsequently mapped to the *C. auris* B8441 reference genome (GenBank accession:
506 GCA_002759435.3) with paired reads counted as one and expression values set to RPKM.
507 Principal component analysis was utilized for the initial clustering assessment of biological
508 replicates and mismatch, insertion, and deletion costs were set to default parameters for RNA-
509 Seq Analysis 2.7. Differential expression was calculated using negative binomial GLM modeling
510 with whole transcriptome RNA-Seq defaults for normalization with Trimmed Mean of M values,
511 using Differential gene expression v1.4 (CLC genomics workbench, Qiagen). Comparisons were
512 made to the wildtype *SKU013* clinical isolate for each condition. Differential expression was
513 defined as fold changes ≥ 2 or ≤ -2 (FDR p-value ≤0.05)
514
515 **Scanning Electron Microscopy**
516 Sterile silicon chips were loaded into 24-well plate and coated overnight with 0.5mL 20%
517 human plasma in carbonate-bicarbonate buffer. Suspensions of SKU013, *Δrba1*::*RBA1*$^{+}$_a , and
518 Δ*rba1_a* were cultured in RPMI-Biofilm media as described above for biofilm production assays
519 with 0.5mL of cells loaded into the wells. Following 24 hour incubation, wells were gently washed
520 with 1mL PBS and biofilms were fixed with 0.1M sodium cacodylate buffer at pH 7.4 with 0.15%
521 alcian blue, 1% tannic acid, 2.5% glutaraldehyde, 2% paraformaldehyde for 2 hours and stored

522 at 4°C. Preparation, staining, and imaging the fixed biofilms was performed by the Electron
523 Microscopy Division of the Cell and Tissue Imaging Center (CTIC-EM) at SJCRH for SEM Fixed
524 biofilms were washed with 0.1M sodium cacodylate buffer + 0.15% alcian blue prior to osmium
525 tetroxide staining in the presence of 0.15% alcian blue. Imaging was performed on a Zeiss
526 GeminiSEM 460. Scale bars were embedded using ImageJ[43].
527
528 **Polystyrene adhesion assay**
529 Adhesion to flat-bottom 96-well non-tissue culture treated polystyrene plates (CS100-
530 701311, NEST SCIENTIFIC) was assessed in RPMI-Growth+ media, defined as RPMI medium
531 1640 + MOPS + 2% dextrose, buffered to pH 7. Adhesion to tissue culture treated plates
532 (TP92696, TPP Midwest Scientific), was assessed for RPMI-Growth+ media and RPMI-Biofilm
533 media in the presence and absence of human plasma, coated as described above. cells cultured
534 and plates were loaded as described for biofilm production assays. Following a 90-minute
535 incubation at 37°C, 250RPM, wells were gently washed once with PBS to remove non-adhered
536 cells. Adhered cells were stained with 100μL of a 10:1 solution of XTT sodium salt and phenazine
537 methosulfate (VWR International LLC). Absorbances at OD_{492} and OD_{630} were read after 60
538 minutes and values were normalized to SKU013.
539
540 **Keratinocyte adhesion assay**
541 Adhesion of *C. auris* to human keratinocytes was determined as previously described[26].
542 Human N/TERT keratinocytes[44] were grown in 96-well plates to complete confluence in
543 keratinocyte-SFM medium (Gibco, 10724-011) supplemented with 30 μg/ml bovine pituitary
544 extract, 0.2 ng/ml epidermal growth factor, and 0.31 mM $CaCl_2$. Overnight *C. auris* cultures were
545 diluted to an OD_{600} of 0.03, and 100 μl of this suspension was added to each well containing
546 keratinocytes. In parallel, an equal volume of culture was added to empty wells, centrifuged (210

547 g, 1 min), and imaged to determine input cell counts, while plates containing keratinocytes were
548 centrifuged under the same conditions and incubated at 37 °C with 5% CO_2 for 1 h. Non-adherent
549 yeast cells were then removed by washing three times with PBS. The remaining cells were fixed
550 in 4% formaldehyde and stained with FITC-conjugated anti-*Candida* antibody (Meridian
551 Bioscience, B65411F; 1:1000). Keratinocyte nuclei and cell bodies were labeled with Hoechst
552 (Thermo Fisher, 62249; 1:1000) and CellMask Deep Red (Thermo Fisher, H32721; 1:5000),
553 respectively.

554 Fluorescent images were acquired at 10X magnification using a BioTek Lionheart FX
555 microscope. The number of adherent *C. auris* cells was quantified using a customized CellProfiler
556 analysis pipeline[26, 45]. Numbers of input cells were determined from brightfield images pre-
557 processed in Fiji/ImageJ (v2.14.0)[43] using a custom macro for edge-based segmentation and
558 binary mask generation. The proportion of adherent to input cells was calculated to assess the
559 adhesion efficiency of each *C. auris* strain.

560

561 **Catheter-Associated Urinary Tract Infection (CAUTI) Modeling**

562 Female C57BL/6 mice (Jackson Laboratory) were subjected to transurethral implantation
563 of a silicone catheter followed by transurethral inoculation of the bladder lumen with ~5×10^5
564 colony forming units (CFU) in PBS, as previously described [32]. Mice were euthanized at 24 hours
565 post-infection by cervical dislocation after anesthesia inhalation and the catheter, bladder,
566 kidneys, spleen, and heart were aseptically harvested. Bladders were weighed and then
567 homogenized for CFUs. The other organs were homogenized, and catheters were cut into small
568 pieces before sonication for fungal CFU enumeration.

569

570 **Statistics and Reproducibility**

571 Statistical parameters and applied analysis methods including exact sample numbers (n)
572 and definitions for representative central value and spread (mean ± SEM, CFU quantifications;

573 representative modal value (n=3), minimum inhibitory concentrations) are annotated in
574 corresponding figure legends. Data from at least three experiments were pooled for each
575 adhesion and biofilm assay and twice for each *in vivo* mouse assay. One-way ANOVA tests, two-
576 tailed Welch's t-tests, and two-tailed Mann-Whitney *U* tests were performed with GraphPad Prism
577 10 software (GraphPad Software) for comparisons of described in-vitro assays and in vivo CAUTI
578 experiments, respectively.

579 For RNA sequencing, statistical analysis was performed using CLC Genomics Workbench
580 version 20.0 (QIAGEN) with paired reads counted as one and expression values set to RPKM.
581 Whole transcriptome differential gene expression analysis was performed with mismatch,
582 insertion, and deletion costs set to default parameters, and a Wald test was used to compare
583 SKU013 against Δ*rba1_a*. Differential expression determined by a fold change of ≥ 2 or ≤ -2 with
584 a False discovery rate (FDR) corrected p value ≤0.05.

585

586 **ACKNOWLEDGMENTS**

587 This work was supported in part by the St. Jude Children's Research Hospital Children's
588 Infection Defense Center and Center for Infectious Diseases Research awards granted to JMR,
589 by the National Institutes of Health (NIH)/ National Institute of Allergy and Infectious Diseases
590 (NIAID) grant U19-AI181767 awarded to TRP, and by the NIH/ NIAID F32 AI181164 awarded to
591 GZ. This work was supported by institutional funds from the University of Notre Dame (to FHST
592 and ALFM), and by grants from the Good Venture Foundation (Open Philanthropy) (to ALFM),
593 from the National Institutes of Health R01AI177875 and R21AI171742 (to FHST), and
594 R01DK128805 (to ALFM). This research included experiments conducted by the Hartwell Center
595 for Bioinformatics & Biotechnology, the St. Jude Center for Advanced Genome Engineering and
596 the Cell and Tissue Imaging Center - Electron Microscopy (CTIC-EM) which are supported in part
597 by ALSAC and the National Cancer Institute at the National Institutes of Health [P30 CA021765].
598 The funders had no role in study design, data collection and interpretation, or the decision to
599 submit the work for publication.

600

601 **AUTHOR CONTIBUTIONS**

602 Conceptualization, J.M.R., T.R.O., F.H.S.T., and A.L.F.M.; methodology, J.M.R., L.A.D., A.A.L.,
603 S.J.J., Q.Z., T.R.O., and A.L.F.M.; Investigation, L.A.D., A.A.L., S.J.J., Q.Z., Q.J.C., and J.M.R.;
604 writing—original draft, L.A.D. and J.M.R.; writing—review & editing, L.A.D., A.A.L., S.J.J., G.Z.,
605 M.A., Q.J.C., S.A., E.M., I.A., W.A., K.A., T.R.O., F.H.S.T., A.L.F.M., and J.M.R.; funding
606 acquisition J.M.R., T.R.O., F.H.S.T., A.L.F.M., and Q.Z.; supervision, T.R.O., F.H.S.T., A.L.F.M.,
607 and J.M.R..

608

REFERENCES

1. World Health Organization. *WHO fungal priority pathogens list to guide research, development and public health action*. (World Health Organization, Geneva, 2022).

2. Satoh K, Makimura K, Hasumi Y, Nishiyama Y, Uchida K, Yamaguchi H. *Candida auris* sp. nov., a novel ascomycetous yeast isolated from the external ear canal of an inpatient in a Japanese hospital. *Microbiol Immunol* **53**, 41-44 (2009).

3. Lockhart SR*, et al.* Simultaneous Emergence of Multidrug-Resistant *Candida auris* on 3 Continents Confirmed by Whole-Genome Sequencing and Epidemiological Analyses. *Clin Infect Dis* **64**, 134-140 (2017).

4. European Centre for Disease Prevention and Control. *Survey on the epidemiological situation, laboratory capacity and preparedness for Candidozyma (Candida) auris, 2024*. (Publications Office of the European Union, 2025).

5. Sabino R, Veríssimo C, Pereira Á A, Antunes F. *Candida auris*, an Agent of Hospital-Associated Outbreaks: Which Challenging Issues Do We Need to Have in Mind? *Microorganisms* **8**, (2020).

6. Baker AD, Gold JAW, Forsberg K, Jones S, Lyman MM. Progression from *Candida auris* Colonization Screening to Clinical Case Status, United States, 2016-2023. *Emerg Infect Dis* **31**, 1613-1617 (2025).

7. Akinbobola AB, Kean R, Hanifi SMA, Quilliam RS. Environmental reservoirs of the drug-resistant pathogenic yeast *Candida auris*. *PLoS Pathog* **19**, e1011268 (2023).

8. Proctor DM*, et al.* Clonal *Candida auris* and ESKAPE pathogens on the skin of residents of nursing homes. *Nature* **639**, 1016-1023 (2025).

9. Pacilli M*, et al.* Regional Emergence of *Candida auris* in Chicago and Lessons Learned From Intensive Follow-up at 1 Ventilator-Capable Skilled Nursing Facility. *Clin Infect Dis* **71**, e718-e725 (2020).

10. Chow NA*, et al.* Multiple introductions and subsequent transmission of multidrug-resistant *Candida auris* in the USA: a molecular epidemiological survey. *The Lancet Infectious Diseases* **18**, 1377-1384 (2018).

11. Codda G*, et al.* In vivo evolution to echinocandin resistance and increasing clonal heterogeneity in *Candida auris* during a difficult-to-control hospital outbreak, Italy, 2019 to 2022. *Euro Surveill* **28**, (2023).

652 12. Rybak JM*, et al.* In vivo emergence of high-level resistance during treatment reveals the
653 first identified mechanism of amphotericin B resistance in *Candida auris*. *Clin Microbiol*
654 *Infect* **28**, 838-843 (2022).

655
656 13. Carolus H*, et al.* Genome-Wide Analysis of Experimentally Evolved *Candida auris* Reveals
657 Multiple Novel Mechanisms of Multidrug Resistance. *mBio* **12**, (2021).

658
659 14. Rybak JM*, et al.* Mutations in *TAC1B*: a Novel Genetic Determinant of Clinical Fluconazole
660 Resistance in *Candida auris*. *mBio* **11**, (2020).

661
662 15. La Bella AA, Santiago-Tirado FH, Flores-Mireles AL. *Candida auris* is emerging as a
663 prevalent urinary pathogen. *PLoS Pathog* **21**, e1013138 (2025).

664
665 16. Chow NA*, et al.* Tracing the Evolutionary History and Global Expansion of *Candida auris*
666 Using Population Genomic Analyses. *mBio* **11**, (2020).

667
668 17. Muñoz JF*, et al.* Clade-specific chromosomal rearrangements and loss of subtelomeric
669 adhesins in *Candida auris*. *Genetics* **218**, (2021).

670
671 18. Barker KS*, et al.* Relative contributions of the *ERG11*$^{(VF125AL)}$ and *MRR1A*$^{(N647T)}$ mutations
672 to fluconazole resistance in Clade III *Candidozyma (Candida) auris* clinical isolates. *Clin*
673 *Microbiol Infect*, (2025).

674
675 19. Rybak JM, Sharma C, Doorley LA, Barker KS, Palmer GE, Rogers PD. Delineation of the
676 Direct Contribution of *Candida auris ERG11* Mutations to Clinical Triazole Resistance.
677 *Microbiol Spectr* **9**, e0158521 (2021).

678
679 20. Mayr EM, Ramírez-Zavala B, Krüger I, Morschhäuser J. A Zinc Cluster Transcription
680 Factor Contributes to the Intrinsic Fluconazole Resistance of *Candida auris*. *mSphere* **5**,
681 (2020).

682
683 21. Massic L*, et al.* Acquired amphotericin B resistance attributed to a mutated *ERG3* in
684 *Candidozyma auris*. *Antimicrob Agents Chemother* **69**, e0060125 (2025).

685
686 22. Doorley LA, Meza-Perez V, Jones SJ, Rybak JM. A *Candidozyma (Candida) auris*-
687 Optimized Episomal Plasmid-Induced Cas9-Editing System Reveals the Direct Impact of
688 the S639F-Encoding *FKS1* Mutation. *J Infect Dis* **232**, e529-e536 (2025).

689
690 23. Spruijtenburg B*, et al.* Whole genome sequencing analysis demonstrates therapy-induced
691 echinocandin resistance in *Candida auris* isolates. *Mycoses* **66**, 1079-1086 (2023).

692

24. Asadzadeh M*, et al.* Molecular characterisation of *Candida auris* isolates from immunocompromised patients in a tertiary-care hospital in Kuwait reveals a novel mutation in *FKS1* conferring reduced susceptibility to echinocandins. *Mycoses* **65**, 331-343 (2022).

25. La Bella AA*, et al.* The catheterized bladder environment promotes Efg1- and Als1-dependent *Candida albicans* infection. *Science Advances* **9**, eade7689 (2023).

26. Zhao G*, et al.* Adhesin Als4112 promotes *Candida auris* skin colonization through interactions with keratinocytes and extracellular matrix proteins. *Nat Commun* **16**, 5673 (2025).

27. Santana DJ*, et al.* A *Candida auris*-specific adhesin, Scf1, governs surface association, colonization, and virulence. *Science* **381**, 1461-1467 (2023).

28. de Assis LJ*, et al.* Nature of β-1,3-Glucan-Exposing Features on *Candida albicans* Cell Wall and Their Modulation. *mBio* **13**, e0260522 (2022).

29. Hopke A, Nicke N, Hidu EE, Degani G, Popolo L, Wheeler RT. Neutrophil Attack Triggers Extracellular Trap-Dependent *Candida* Cell Wall Remodeling and Altered Immune Recognition. *PLoS Pathog* **12**, e1005644 (2016).

30. Yang M*, et al.* Control of β-glucan exposure by the endo-1,3-glucanase Eng1 in *Candida albicans* modulates virulence. *PLoS Pathog* **18**, e1010192 (2022).

31. Louvet M*, et al.* Ume6-dependent pathways of morphogenesis and biofilm formation in Candida auris. *Microbiol Spectr* **12**, e0153124 (2024).

32. Conover MS, Flores-Mireles AL, Hibbing ME, Dodson K, Hultgren SJ. Establishment and Characterization of UTI and CAUTI in a Mouse Model. *J Vis Exp*, e52892 (2015).

33. Escandón P*, et al.* Notes from the Field: Surveillance for *Candida auris* - Colombia, September 2016-May 2017. *MMWR Morb Mortal Wkly Rep* **67**, 459-460 (2018).

34. Barbian HJ*, et al. Candida auris* Outbreak and Epidemiologic Response in Burn Intensive Care Unit, Illinois, USA, 2021-2023. *Emerg Infect Dis* **31**, 438-447 (2025).

35. Rhodes J*, et al.* Genomic epidemiology of the UK outbreak of the emerging human fungal pathogen *Candida auris*. *Emerg Microbes Infect* **7**, 43 (2018).

36. Araúz AB*, et al.* Isolation of *Candida auris* from 9 patients in Central America: Importance of accurate diagnosis and susceptibility testing. *Mycoses* **61**, 44-47 (2018).

37. Chowdhary A*, et al.* New clonal strain of Candida auris, Delhi, India. *Emerg Infect Dis* **19**, 1670-1673 (2013).

38. Gorzalski A*, et al.* The use of whole-genome sequencing and development of bioinformatics to monitor overlapping outbreaks of Candida auris in southern Nevada. *Front Public Health* **11**, 1198189 (2023).

39. Mishra A, Aggarwal A, Khan F. Medical Device-Associated Infections Caused by Biofilm-Forming Microbial Pathogens and Controlling Strategies. *Antibiotics (Basel)* **13**, (2024).

40. Molina JJ, Flores-Mireles AL. CAUTIon - not all UTIs are the same. *Nat Rev Urol* **22**, 799-814 (2025).

41. Ahmad S, Khan Z, Al-Sweih N, Alfouzan W, Joseph L. *Candida auris* in various hospitals across Kuwait and their susceptibility and molecular basis of resistance to antifungal drugs. *Mycoses* **63**, 104-112 (2020).

42. Gulati M*, et al.* In Vitro Culturing and Screening of *Candida albicans* Biofilms. *Curr Protoc Microbiol* **50**, e60 (2018).

43. Schindelin J*, et al.* Fiji: an open-source platform for biological-image analysis. *Nat Methods* **9**, 676-682 (2012).

44. Dickson MA*, et al.* Human keratinocytes that express hTERT and also bypass a p16(INK4a)-enforced mechanism that limits life span become immortal yet retain normal growth and differentiation characteristics. *Mol Cell Biol* **20**, 1436-1447 (2000).

45. Lamprecht MR, Sabatini DM, Carpenter AE. CellProfiler: free, versatile software for automated biological image analysis. *Biotechniques* **42**, 71-75 (2007).

46. Khan Z, Ahmad S, Al-Sweih N, Joseph L, Alfouzan W, Asadzadeh M. Increasing prevalence, molecular characterization and antifungal drug susceptibility of serial *Candida auris* isolates in Kuwait. *PLoS One* **13**, e0195743 (2018).

47. Al-Obaid I*, et al.* Fatal Breakthrough Candidemia in an Immunocompromised Patient in Kuwait Due to *Candida auris* Exhibiting Reduced Susceptibility to Echinocandins and Carrying a Novel Mutation in Hotspot-1 of FKS1. *J Fungi (Basel)* **8**, (2022).

48. Alfouzan W*, et al.* Molecular Epidemiology of *Candida auris* Outbreak in a Major Secondary-Care Hospital in Kuwait. *J Fungi (Basel)* **6**, (2020).

FIGURES

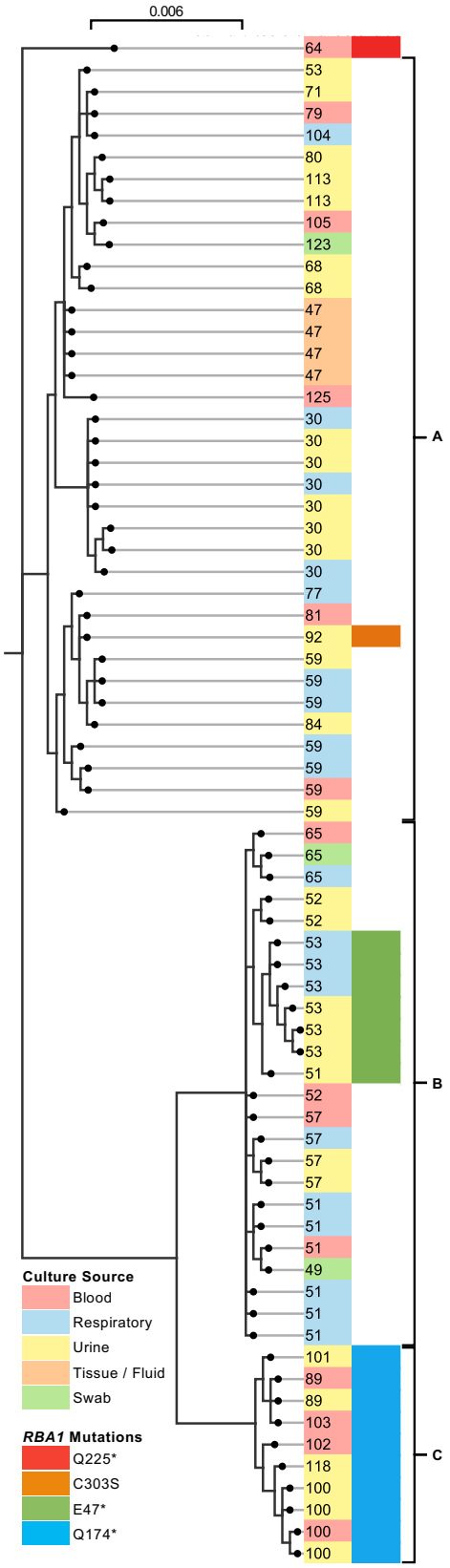

Fig 1. Clinical emergence and spread of *C. auris* isolates harboring mutations in *RBA1* during an outbreak of infections.
Phylogenetic analysis of 70 isolates from documented outbreaks of *C. auris* infections in Kuwait. Nodes indicate branch length termination. Patient cases, culture sources, and *RBA1* mutations are indicated on the right.

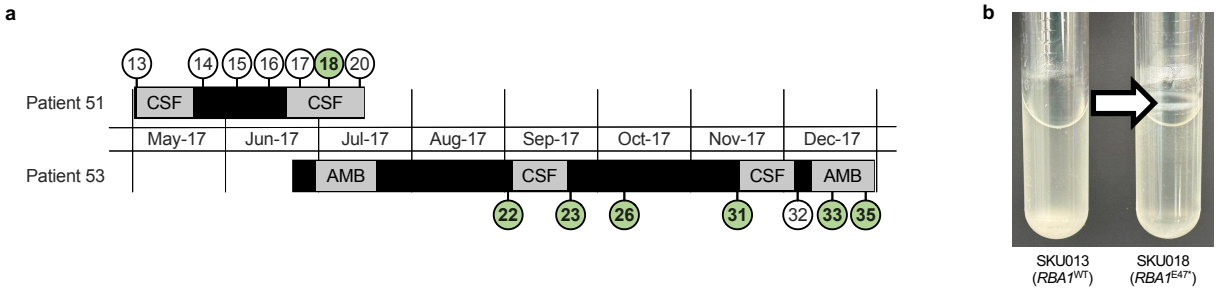

c

	Culture Source	SNPs vs SKU013	*RBA1*	Susceptibility FLU	AmB	Echino
Patient 51						
SKU013	Endotracheal asp.	-	WT	**R**	S	S
SKU014	Endotracheal asp.	2	WT	**R**	S	S
SKU015	Endotracheal asp.	4	WT	**R**	S	S
SKU016	Endotracheal asp.	4	WT	**R**	S	S
SKU017	Endotracheal asp.	4	WT	**R**	S	S
SKU018	Urine	8	**E47***	**R**	S	**R**
SKU020	Blood	5	WT	**R**	S	S
Patient 53						
SKU022	Endotracheal asp.	6	**E47***	**R**	S	S
SKU023	Endotracheal asp.	6	**E47***	**R**	S	S
SKU026	Tracheal sec.	7	**E47***	**R**	S	S
SKU031	Urine	7	**E47***	**R**	**R**	S
SKU032	Urine	89	WT	**R**	S	S
SKU033	Urine	8	**E47***	**R**	**R**	S
SKU035	Urine	8	**E47***	**R**	S	**R**

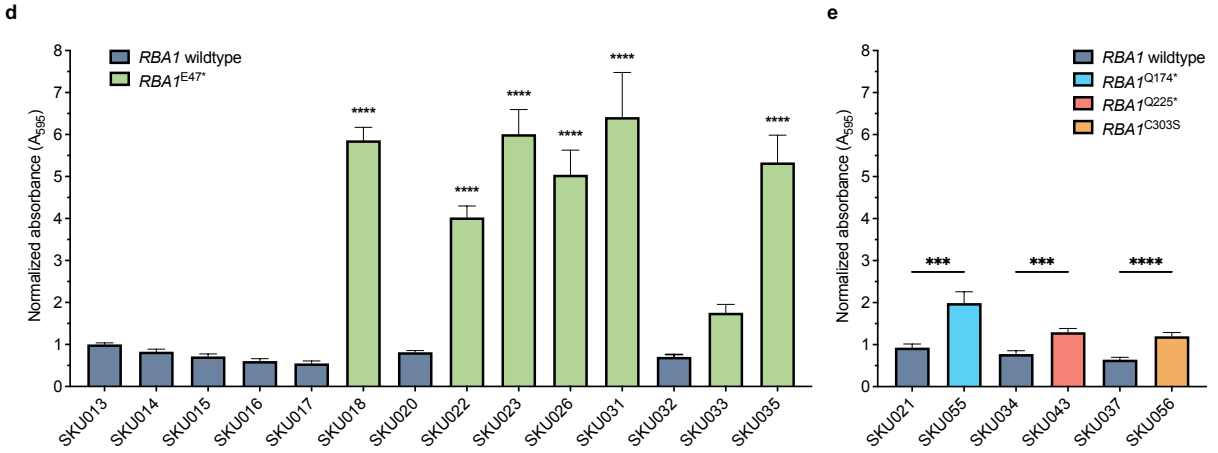

Fig 2. *RBA1* mutations emerge during patient infection and are associated with increased biofilm production. a, Timeline of patient cases 51 and 53 with *C. auris* isolations and antifungal treatment courses indicated, AMB: liposomal amphotericin B, CSF: caspofungin. Isolate numbers (SKU) with *RBA1*^{E47*} mutations indicated by green background. **b,** Biofilm formation on sidewall of polystyrene (PS) tubes following overnight growth in RPMI culture media. Arrow indicates visible biofilm ring. **c,** Isolate details including name, culture source, number of coding region single nucleotide polymorphisms (SNPs) relative to the earliest isolate SKU013, *RBA1* genotype, and interpretation of susceptibility to fluconazole (FLU), amphotericin B (AmB), and echinocandins (Echino) based on current CDC tentative breakpoints. **d, e,** Biofilm production of isolates formed over 48 hours on fibrinogen-treated PS in urine media supplemented with 10% serum. Biofilm assessment via crystal violet staining with absorbance read at 595 nm. Reads were normalized to the initial isolate SKU013 with means (bars) and standard error of the means plotted in GraphPad Prism. (**d**) gray-blue bars indicate wildtype *RBA1* containing isolates and green indicates *RBA1*^{E47*} mutation. Clinical isolates harboring (**e**) *RBA1*^{Q174*}, *RBA1*^{Q225*}, and *RBA1*^{C303S} mutations are indicated with light blue, red and orange bars, respectively, and plotted alongside a corresponding closest genetic relative harboring a wildtype *RBA1* (gray-blue bars). Kruskal-Wallis statistical one-way ANOVA testing with Dunn's correction for multiple comparisons showed significant differences between SKU013 and *RBA1*^{E47*} containing isolates (**d**; ****P = <0.0001) and *RBA1*^{Q174*}, *RBA1*^{Q225*}, and *RBA1*^{C303S} isolates and corresponding closest genetic relative (**e**; ***P= <0.001).

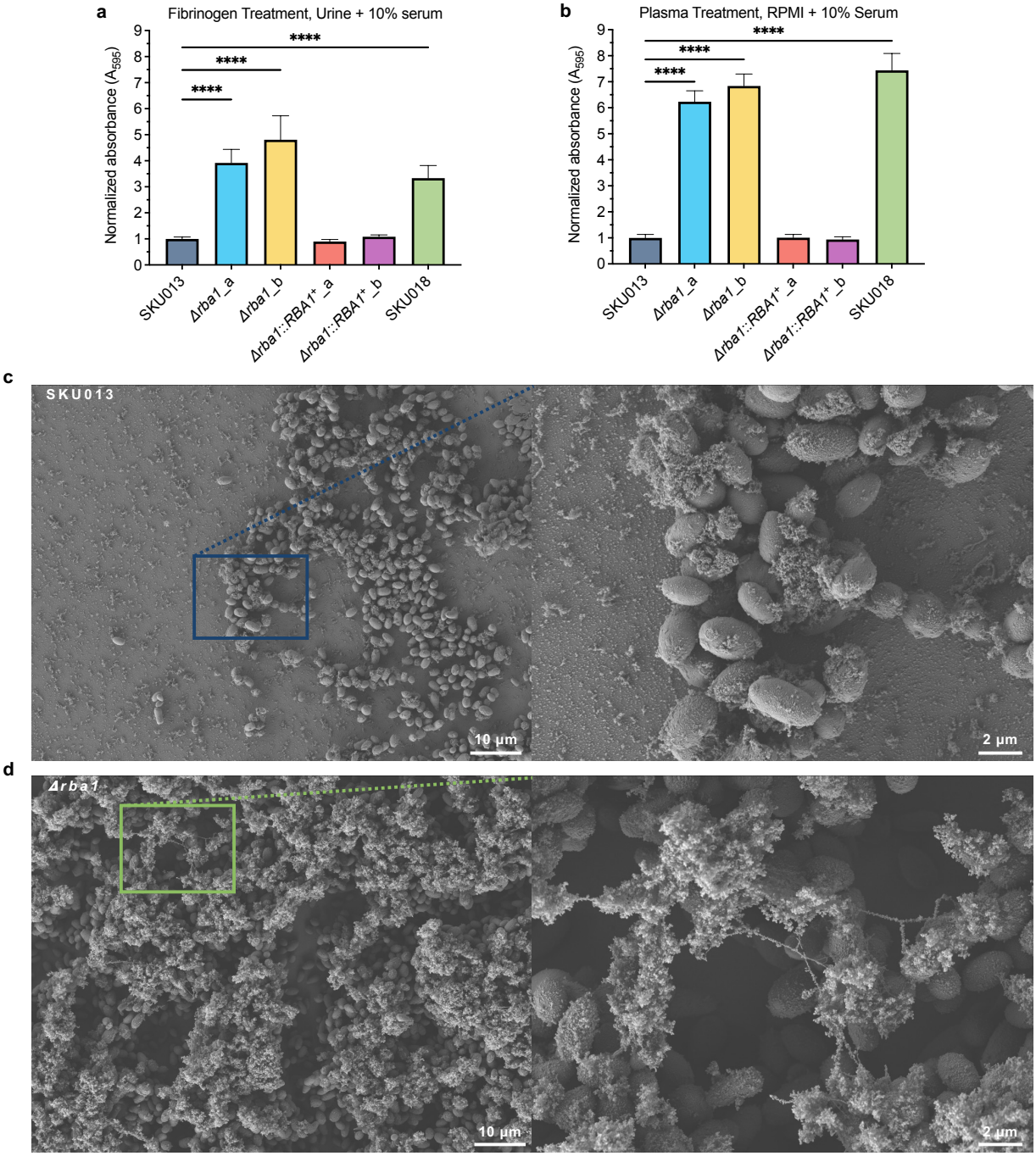

Fig 3. Loss of *RBA1* enhances biofilm production

a,b, Biofilm production of *C. auris RBA1* strains formed on (**a**) fibrinogen coated microtiter plates in human urine media supplemented with 10% human serum after 48hrs and (**b**) on human plasma coated microtiter plates in RPMI tissue culture media supplemented with 10% human serum after 24hrs. Biofilms stained with crystal violet and absorbance measured at 595 nm. Absorbance reads were normalized to SKU013 (*RBA1*^{WT}) and graphed (GraphPad Prism) showing mean (bars) and standard error of the mean. Kruskal-Wallis statistical testing with Dunn's correction for multiple comparisons showed significant differences between *Δrba1_a, Δrba1_b*, and SKU018 (*RBA1*^{E47*}) when compared to SKU013 (*RBA1*^{WT}) (****P= <0.0001). **c, d,** Representative SEM images for (**c**) SKU013 (*RBA1*^{WT}) and (**d**) *Δrba1* biofilms formed over 24 hours in RPMI media supplemented with 10% human serum on silicone disks treated with human plasma. Dried samples coated with 5nm iridium and imaged in the Zeiss Gemini 460 (CITC-SJCRH) using Secondary Electrons detector at 2kV, 77pA, and 5mm working distance.

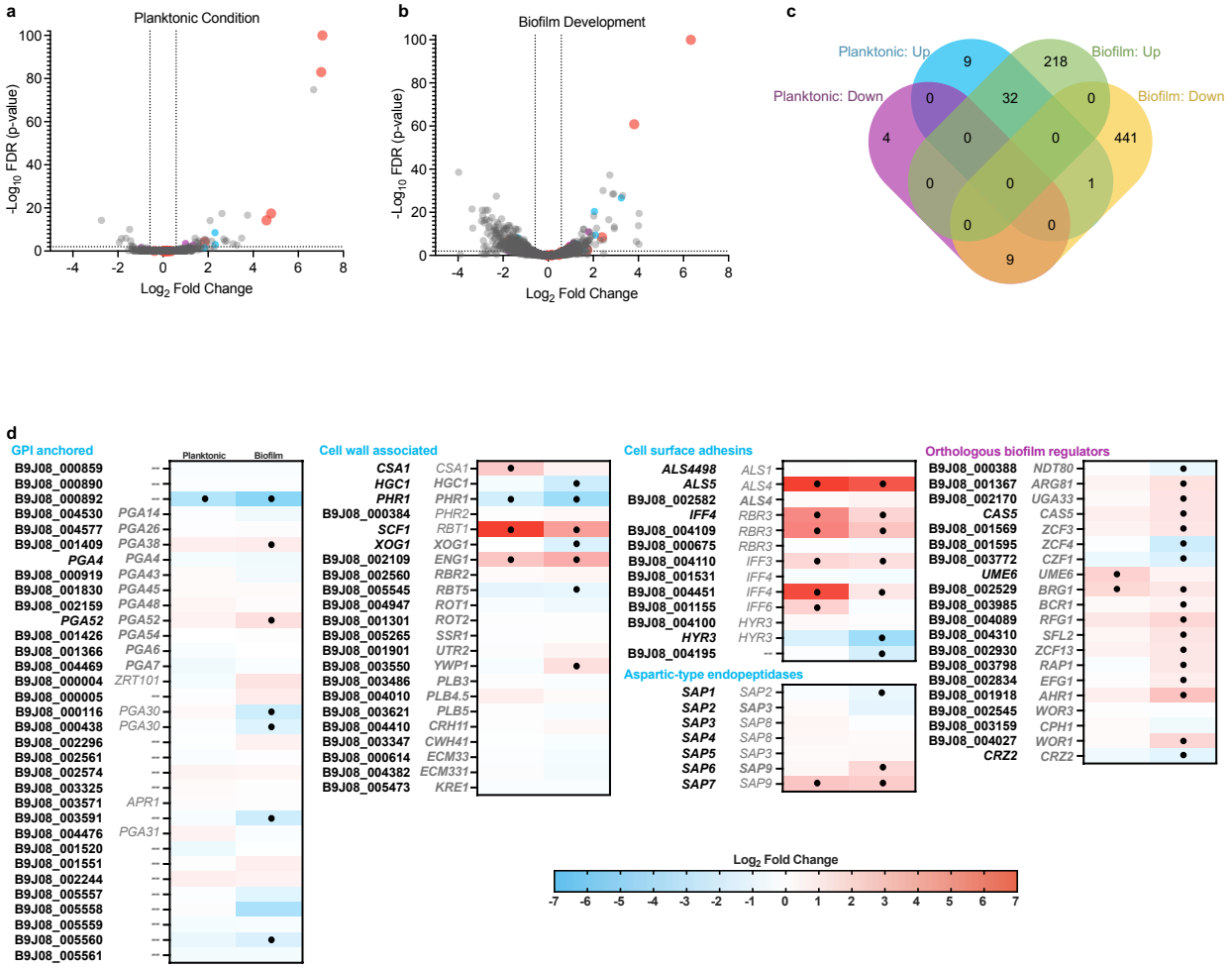

Fig 4. Loss of *RBA1* increases expression of *C. auris* adhesins and virulence factors under both planktonic and biofilm conditions.

a,b Volcano plot of differentially expressed genes between clinical isolate SKU013 and *Δrba1* strain during exponential growth phase when cultured under (a) planktonic growth conditions (10mL RPMI media in 50mL conical tube incubated at 35°C with 220RPM) and (**b**) biofilm-forming conditions (10mL RPMI media in plasma-treated T75 flasks for static incubation at 37°C). Blue, purple, and red highlighted dots represent cell wall associated, ZCF, and cell aggregation or biofilm formation encoding genes, respectively. Dotted lines represent lower limit equivalents for fold changes of ≥ |1.5| on the x-axis, and a false discovery rate (FDR) p-value ≤0.05 on the y-axis. **c**, Venn diagram comparing differentially expressed genes (≥ |1.5| on the x-axis, and a false discovery rate p-value ≤0.05) exhibiting up-regulation or down-regulation in the *Δrba1* strain under planktonic or biofilm growth conditions. **d**, Differential gene expression encoding predicted GPI-anchored proteins, cell surface adhesions, fungal cell wall associated proteins, aspartic-type endopeptidases, and genes orthologous to transcriptional regulators of biofilm formation in *Candida albicans* with planktonic expression on the left and biofilm expression on the right for each column. *C. albicans* genes are listed in gray with true orthologs bolded. Significant differential expression (fold change ≥ |1.5|; FDR p-value ≤ 0.05) is indicated with a black dot.

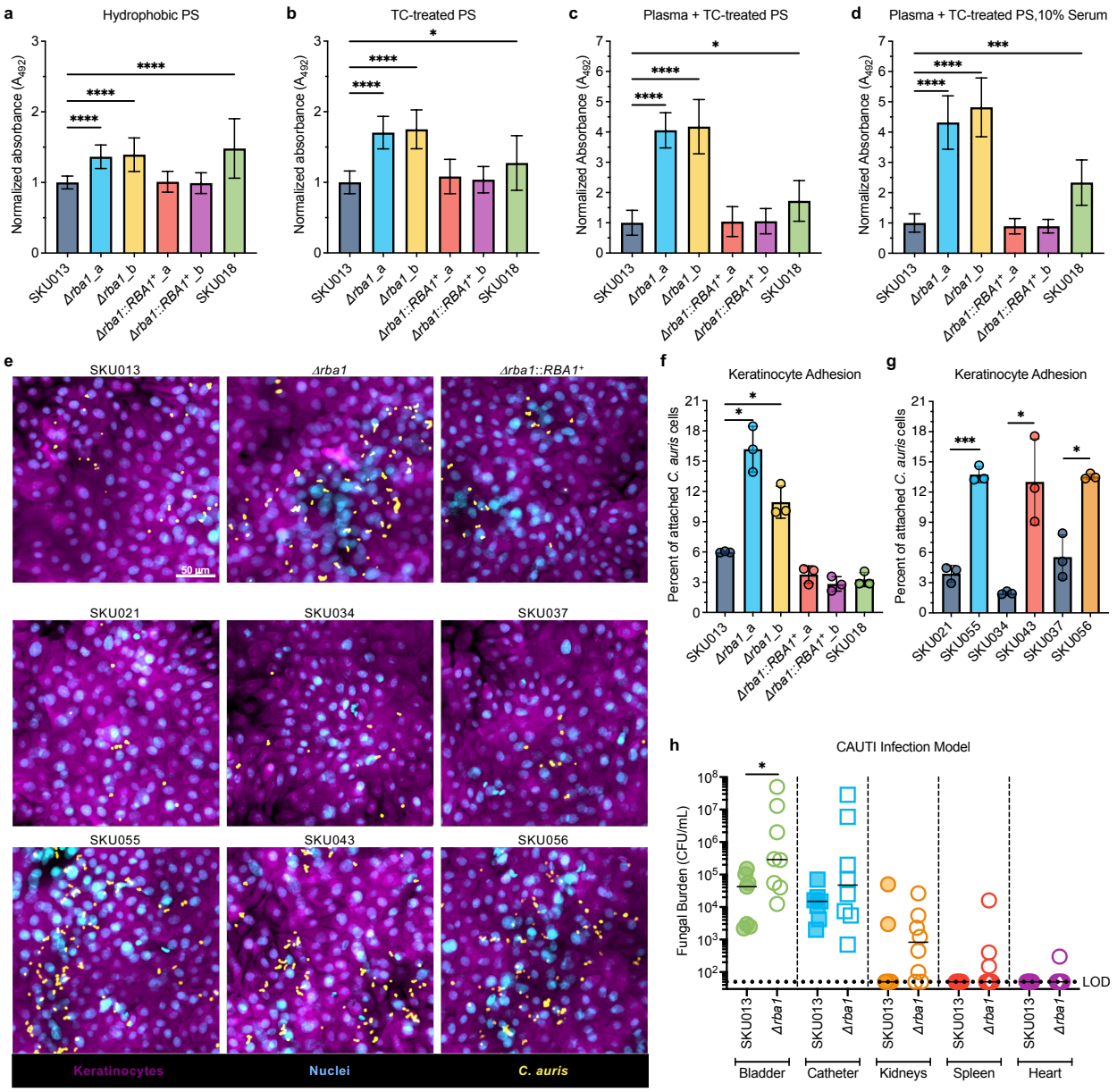

Fig 5. Loss of *RBA1* increases adhesion and fungal burden in murine CAUTI model. **a, b, c, d,** Adhesion of *C. auris* isolates and *RBA1* strains grown in RPMI culture media after 90 minutes to (**a**) untreated polystyrene (PS), (**b**) tissue culture (TC) -treated PS, (**c**) human plasma coated, TC-treated PS, and (**d**) human plasma coated, TC-treated PS grown in RPMI supplemented with 10% human serum. Adhesion assessed by absorbance at 490 nm following XTT treatment. Statistical significance was determined using Kruskal-Wallis one-way ANOVA tests followed by a Dunn's test for multiple comparisons to the *RBA1*^{WT} control SKU013 (*$P \leq 0.05$; ****$P < 0.0001$). **e,** Representative immunofluorescence images showing adherence of *C. auris* cells to human N/TERT keratinocytes. *C. auris* was stained with FITC-conjugated anti-*Candida* antibody (yellow) and keratinocytes were stained using CellMask Deep Red (magenta) with a Hoechst counterstain for nuclei identification (blue). **f, g,** Quantification of *C. auris* isolates strains adhered to human N/TERT keratinocytes as measured by the proportion of attached cells remaining after washing. Bars represent mean ± standard deviation for three biological replicates. Statistically significant adhesion increases were determined using unpaired two-tailed Welch's t-tests for (**e**) *Δrba1* compared to SKU013 (*$P \leq 0.05$) and (**g**) SKU055 (*RBA1*^{Q174*}), SKU043 (*RBA1*^{Q225*}), and SKU056 (*RBA1*^{C303S}) compared to *RBA1*^{WT} isolates, SKU021, SKU034, and SKU037, respectively (*$P \leq 0.05$; ***$P \leq 0.001$). **i**, Fungal burden of SKU013 and the derivative *Δrba1* strain obtained from the catheter material or bladder, kidney, spleen, and heart tissues after infection in a murine model of catheter associated urinary tract infection (CAUTI). Two-tailed Mann-Whitney tests showed significant differences in fungal burden recovered from bladder tissue (*$P \leq 0.05$, n=8 mice per group). CFU, colony forming units; LOD, lower limit of detection.

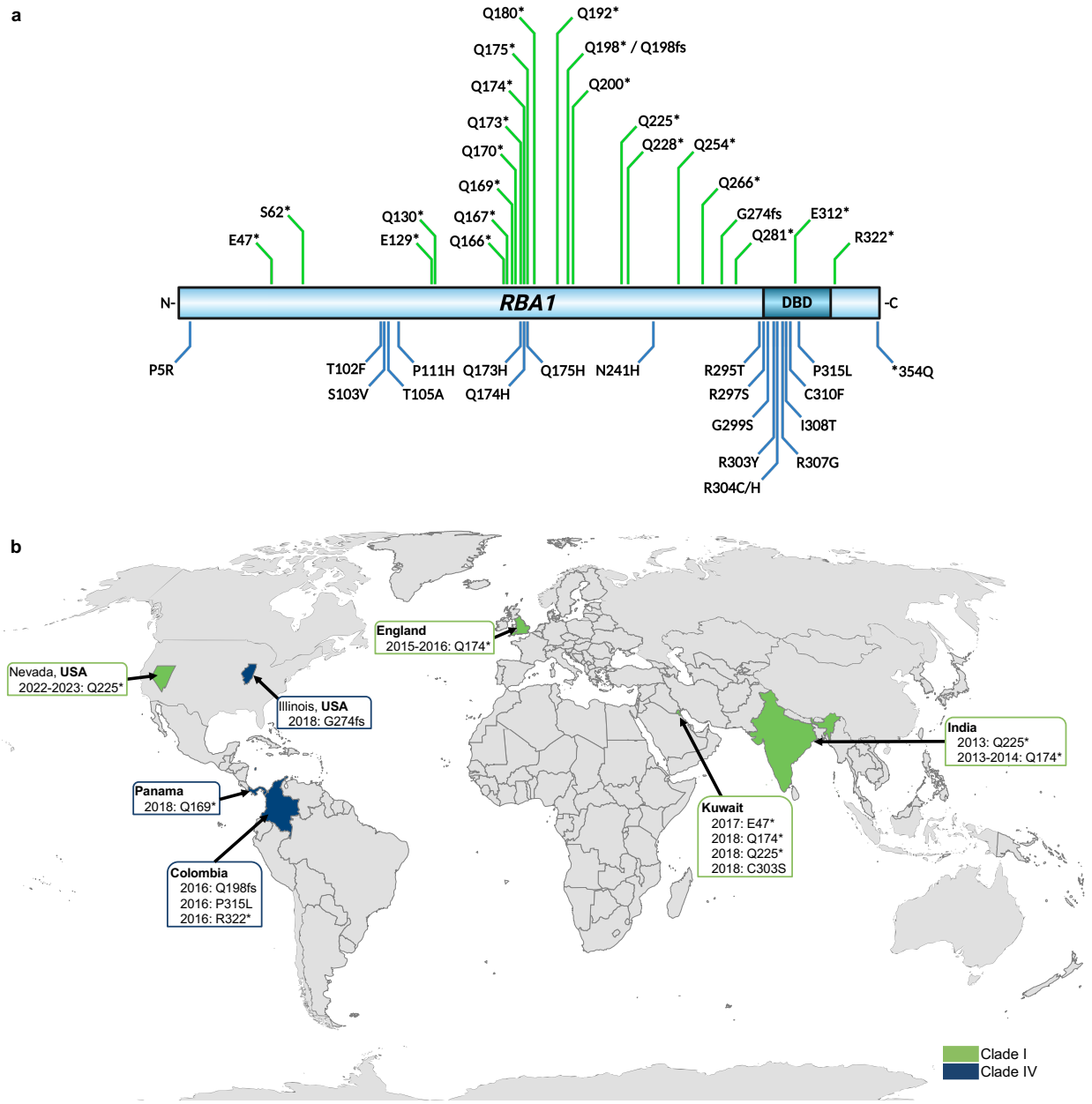

Fig 6. Identification of *RBA1* mutations emerging during numerous outbreaks of *C. auris* infections worldwide.

a, Diagram depicting non-synonymous mutations in *RBA1* identified by analyzing publicly available *C. auris* whole genome sequencing data. Green lines on top of figure indicate early stop codons and frameshift mutations. Blue lines on bottom of figure indicate missense mutations. N241H and *354Q were identified among all clinical isolates classified as clade IV. DBD: DNA-binding domain. **b,** World map indicating locations of documented outbreaks of *C. auris* infections where mutations in *RBA1* were identified from publicly available data. Green fills indicate isolates representing genetic Clade I and blue fills indicate isolates representing genetic clade IV.

871 **SUPPLEMENTAL DATA**

872 **Patient 51 and 53 Case Descriptions:**

873 Patient 51 was a 54-year-old male with a past medical history significant for multiple
874 myeloma admitted to the intensive care unit (ICU) of Hospital F, a tertiary care center associated
875 with Kuwait Cancer Control Center in Kuwait which cares for immunocompromised patients
876 including cancer patients, burn patients and transplant recipients diagnosed and requiring
877 treatment for infectious diseases. Patient 51 was receiving a 14-day course of empiric
878 caspofungin treatment when *C. auris* isolate SKU013 (*RBA1*^{WT}; wildtype-*RBA1*) was first
879 identified from a culture of their endotracheal tube and considered to represent colonization
880 (**Fig. 2a**). Four successive isolates (**Fig. 2c**) were identified from endotracheal tube cultures, and
881 the presence of respiratory symptoms prompted a 21-day course of empiric caspofungin
882 treatment. During this treatment, isolate SKU018 (*RBA1*^{E47*}) was obtained from the patient's
883 urinary catheter. SKU018 notably exhibited *in vitro* resistance to echinocandins (*FKS1*^{S639F}),
884 although it was still thought to represent likely colonization. SKU020 was obtained from a blood
885 culture the day before patient 51 expired. SKU020 also exhibited elevated *in vitro* echinocandin
886 resistance and differed from the earlier respiratory tract isolates SKU016 and SKU017 by only
887 one coding region SNP (*FKS1*^{R1354H}), indicating likely dissemination from the respiratory tract.

888 Patient 53 was a 33-year-old female in the ICU of the same tertiary care hospital (Hospital
889 F) with a significant past medical history for Hodgkin's lymphoma and advanced stage nodular
890 sclerosis. Approximately one month after receiving a 21-day empiric course of liposomal
891 amphotericin B (AmB) for suspected respiratory infection, the patient's respiratory condition
892 worsened and *C. auris* (SKU022) was isolated from the patient's endotracheal tube. Notably,
893 isolate SKU022 harbored the same *RBA1*^{E47*} mutation present in the isolate previously cultured
894 from the urine of patient 51 (SKU018), and genetically these two isolates differed by four coding
895 region SNPs, suggestive of pathogen lateral transmission. Following completion of a 14-day
896 course of caspofungin treatment, two subsequent *C. auris* isolates (both *RBA1*^{E47*}) were cultured

897 from endotracheal tube and tracheal aspirate cultures, prompting a second 14-day course of
898 liposomal AmB. After this second course of AmB, all cultures from respiratory sources remained
899 negative. However, one month later the patient was suspected to have developed a CAUTI and
900 urine cultures yielded isolate SKU031 (*RBA1*^{E47*}). A second 14-day course of caspofungin was
901 initiated after SKU031 was found to be AmB-resistant. Subsequently, AmB-susceptible *C. auris*
902 (SKU032) was cultured from the patient's urine and a third course of liposomal AmB was given.
903 During this third course of AmB, two additional isolates were obtained from urine cultures,
904 SKU033 (*RBA1*^{E47*}) and SKU035 (*RBA1*^{E47*}), and exhibited decreased susceptibility to AmB and
905 echinocandins, respectively. Patient 53 was then transferred to another care facility, precluding
906 further follow-up.
907

908 **Supplemental Table 1. *Candidozyma auris* isolates and strains**

CLINICAL ISOLATES

SKU_ID	Mycology Reference Laboratory ID	Patient ID	Subclade	Isolation source	Previous citations
SKU001	Kw1983-16	47	Ic	Tissue	[46]
SKU002	Kw2031-16	47	Ic	Ab. drain fluid	[46]
SKU003	Kw2236-16	47	Ic	Pus	[46]
SKU004	Kw2254-16	47	Ic	Tissue	[46, 24]
SKU005	Kw2442-16	30	Ic	Urine	[23, 46]
SKU006	Kw2515-16	30	Ic	Tracheal sec.	[23, 46]
SKU007	Kw2555-16	30	Ic	Urine	[23, 46]
SKU008	Kw369-17	30	Ic	Tracheal sec.	[23, 46]
SKU009	Kw1138-17	30	Ic	Urine	[23, 46]
SKU010	Kw1239-17	30	Ic	Urine	[23, 46]
SKU011	Kw1308-17	30	Ic	Urine	[23, 46]
SKU012	Kw1388-17	30	Ic	Tracheal sec.	[23, 46]
SKU013	Kw1432-17	51	Ib	ETT	[46, 24, 23]
SKU014	Kw1695-17	51	Ib	Tracheal aspirate	[46, 24]
SKU015	Kw1825-17	51	Ib	Tracheal aspirate	[46, 24]
SKU016	Kw1856-17	51	Ib	Tracheal aspirate	[46, 24]
SKU017	Kw1893-17	51	Ib	ETT	[46, 24, 23]
SKU018	Kw1994-17	51	Ib	Urine	[46, 24, 23]
SKU019	Kw2040-17	49	Ib	Vaginal swab	[46, 24]
SKU020	Kw2074-17	51	Ib	Blood	[46, 24, 23]
SKU021	Kw2260-17	52	Ib	Blood	[46, 24, 23]
SKU022	Kw2501-17	53	Ib	ET aspirate	[46, 24, 23]
SKU023	Kw2647-17	53	Ib	ET aspirate	[46, 24]
SKU024	Kw2713-17	52	Ib	Urine	[46, 24, 23]
SKU025	Kw2742-17	52	Ib	Urine	[24, 23]
SKU026	Kw2871-17	53	Ib	Tracheal sec.	[24]
SKU027	Kw2968-17	57	Ib	Urine	[24]
SKU028	Kw2989-17	57	Ib	ETT	[24]
SKU029	Kw3092-17	57	Ib	Catheter tip	[24, 23]
SKU030	Kw3134-17	57	Ib	Urine	[24, 23]
SKU031	Kw3135-17	53	Ib	Urine	[24, 23]
SKU032	Kw3367-17	53	Ib	Urine	[24]
SKU033	Kw3424-17	53	Ib	Urine	[24, 23]
SKU034	Kw3506-17	59	Ic	Urine	[47]
SKU035	Kw3521-17	53	Ib	Urine	[24, 23]
SKU036	Kw3525-17	59	Ic	Tracheal sec.	[47]

SKU037	Kw3584-17	59	Ic	Urine	[47]
SKU038	Kw55-18	65	Ib	Sputum	[24], [23]
SKU039	Kw60-18	59	Ic	Tracheal sec.	[23], [47]
SKU040	Kw87-18	59	Ic	Blood	[23], [47]
SKU041	Kw93-18	59	Ic	Tracheal sec.	[23], [47]
SKU042	Kw108-18	59	Ic	Tracheal sec.	[23], [47]
SKU043	Kw137-18	64	Ic	Blood	[41]
SKU044	Kw147-18	65	Ib	Blood	[24], [23]
SKU045	Kw257-18	68	Ic	Urine	[41]
SKU046	Kw334-18	65	Ib	Oral swab	[24], [23]
SKU047	Kw532-18	71	Ic	Urine	[41]
SKU048	Kw1014-18	79	Ic	Blood	[41]
SKU049	Kw1148-18	80	Ic	Urine	[41]
SKU050	Kw1201-18	77	Ic	Bronchial washing	[41]
SKU051	Kw1252-18	81	Ic	Blood	[41]
SKU052	Kw1517-18	68	Ic	Urine	[41]
SKU053	Kw1610-18	84	Ic	Urine	[41]
SKU054	Kw1674-18	89	Ib	Urine	[24]
SKU055	Kw1753-18	89	Ib	Blood	[24]
SKU056	Kw2103-18	92	Ic	Urine	[41]
SKU057	Kw2201-18	100	Ib	Urine	[41]
SKU057	Kw2201-18	100	Ib	Urine	[41]
SKU058	Kw2272-18	102	Ib	Blood	[41]
SKU059	Kw2427-18	103	Ib	Blood	[48]
SKU060	Kw2466-18	105	Ic	Blood	[41]
SKU061	Kw2518-18	101	Ib	Urine	[41]
SKU062	Kw2570-18	100	Ib	Urine	[41]
SKU063	Kw2717-18	104	Ic	Tracheal sec.	[41]
SKU064	Kw2821-18	100	Ib	Urine	[41]
SKU065	Kw2885-18	100	Ib	Blood	[41]
SKU066	Kw2898-18	113	Ic	Urine	[41]
SKU067	Kw2999-18	113	Ic	Urine	[41]
SKU068	Kw3014-18	118	Ib	Urine	[41]
SKU069	Kw3144-18	125	Ic	Blood	[41]
SKU070	Kw3204-18	123	Ic	Groin swab	[41]

Strain ID	**Background**	***RBA1* Genotype**	**Citations**
*Δrba1*_a	SKU013	B9J08_003209:c.950CAGT>CTTAT	This study
*Δrba1*_b	SKU013	B9J08_003209:c.950CAGT>CTTAT	This study
Δrba1::RBA1^{+}_a	*Δrba1*_b	*RBA1*^{WT}	This study
Δrba1::RBA1^{+}_b	*Δrba1*_a	*RBA1*^{WT}	This study

909 **Supplemental Table 2. Oligos and Primers**

Name	Sequence	Notes
RBA1_RT_AMP-F	CGCCAATCCATGTAACCCTC	Amplify Repair Template sequence: *Δrba1_RT-gBlock* for *Δrba1;* SKU013 genomic DNA for *RBA1*$^{+}$
RBA1_RT_AMP-R	GTTGTTGTTGGATATGAGGTGG	
Δrba1_gRNA_TOP	CCACAGCACGGGGTGAGCCAGTC	Guide sequences inserted into pJMR19 for *Δrba1* in SKU013
Δrba1_gRNA_BOT	AACGACTGGCTCACCCCGTGCTG	
RBA1^{+}*_gRNA_TOP*	CCACTGGACTCGAGCCCCAGATA	Guide sequences inserted into pJMR19 for *RBA1*$^{+}$in *Δrba1*
RBA1^{+}*_gRNA_BOT*	AACTATCTGGGGCTCGAGTCCAG	
*RBA1*_scn_F	CCGACCCTTGTTCCCTCCTC	PCR Amplification of *RBA1* for Screening
*RBA1*_scn_R	GTGGGAGACCGGCGTTG	
RBA1_SeqF	CCTACCTCCTCCATGCCC	Sanger Sequencing Primer
Δrba1_RT-gBlock	TTCGGTGTCTGAGTTGATTGTGGGCGCCCAGCTCTCGTCCCACCTCGACCGCTCTCCTAACCACATGACAGTGAAGCACCTGGACTCGAGCCCCAGATAAGGCTCACCCCGTGCTGCCTCACCTGGAAAAAAGCACTTTTGCCTCCTCGGTGCCGCCGCCTCTGGCGCCCTCGTTACATCCACCCGTGGCGTTTCC	Repair template gBlock for *Δrba1* in SKU013

910
911

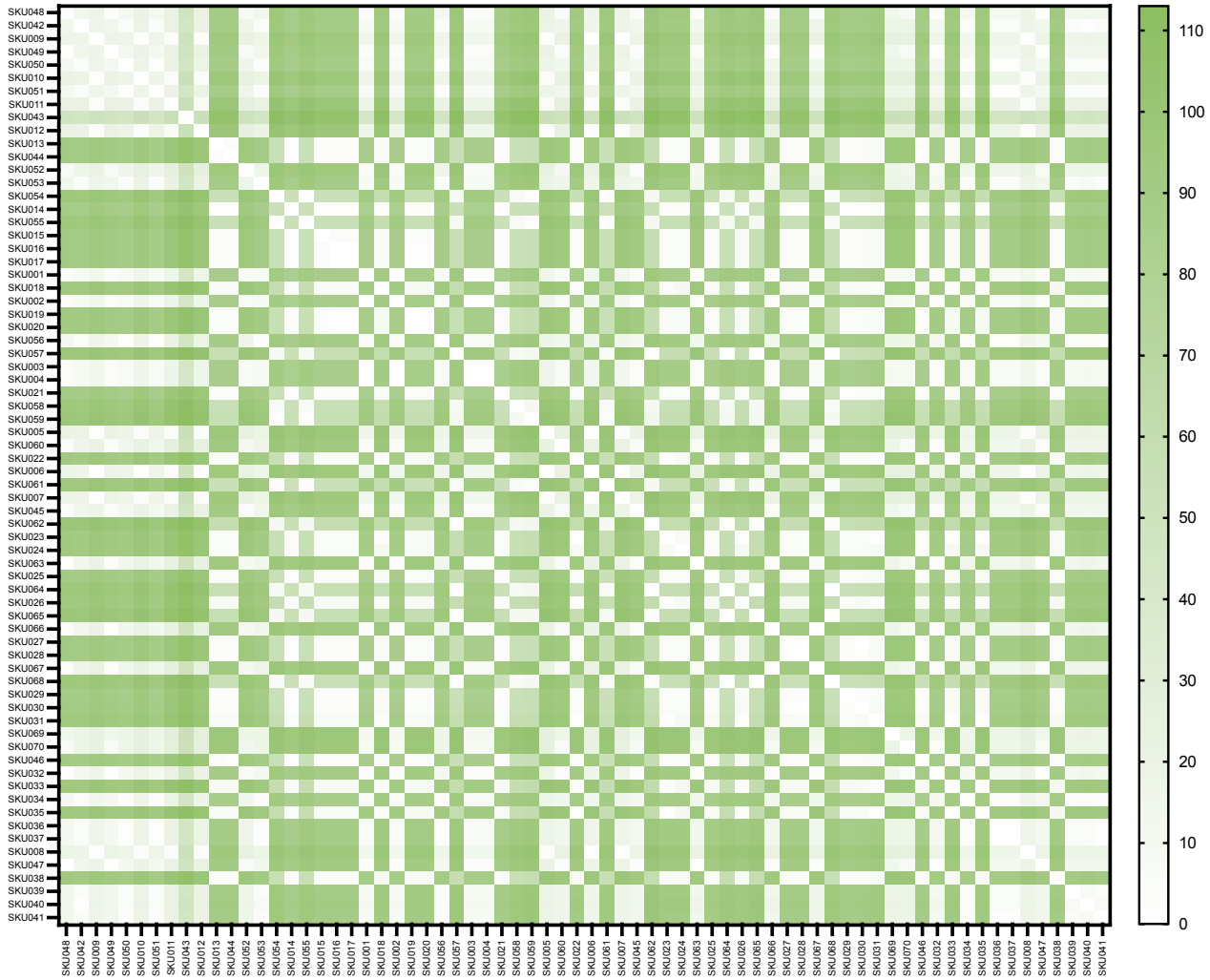

Supplementary Figure 1. Matrix of identified single nucleotide polymorphisms (SNP) in coding regions of genome. *C. auris* isolate Genomes aligned to reference genome GCA002759435.3 (clade I, B8441_v3) for SNP identifications. SNP calling performed with fixed ploidy variant detection in CLC genomics workbench (Qiagen). 46,231 SNPs identified among the annotated open reading frame with identification of 46,055 SNPs leading to amino acid changes across all isolates.

920
921 **SUPPLEMENTAL REFERENCES**
922

923 1. Khan Z, Ahmad S, Al-Sweih N, Joseph L, Alfouzan W, Asadzadeh M. Increasing
924 prevalence, molecular characterization and antifungal drug susceptibility of serial *Candida*
925 *auris* isolates in Kuwait. *PLoS One* **13**, e0195743 (2018).

926
927 2. Asadzadeh M*, et al.* Molecular characterisation of *Candida auris* isolates from
928 immunocompromised patients in a tertiary-care hospital in Kuwait reveals a novel mutation
929 in *FKS1* conferring reduced susceptibility to echinocandins. *Mycoses* **65**, 331-343 (2022).

930
931 3. Spruijtenburg B*, et al.* Whole genome sequencing analysis demonstrates therapy-induced
932 echinocandin resistance in *Candida auris* isolates. *Mycoses* **66**, 1079-1086 (2023).

933
934 4. Al-Obaid I*, et al.* Fatal Breakthrough Candidemia in an Immunocompromised Patient in
935 Kuwait Due to *Candida auris* Exhibiting Reduced Susceptibility to Echinocandins and
936 Carrying a Novel Mutation in Hotspot-1 of *FKS1*. *J Fungi (Basel)* **8**, (2022).

937
938 5. Ahmad S, Khan Z, Al-Sweih N, Alfouzan W, Joseph L. *Candida auris* in various hospitals
939 across Kuwait and their susceptibility and molecular basis of resistance to antifungal
940 drugs. *Mycoses* **63**, 104-112 (2020).

941
942 6. Alfouzan W*, et al.* Molecular Epidemiology of *Candida auris* Outbreak in a Major
943 Secondary-Care Hospital in Kuwait. *J Fungi (Basel)* **6**, (2020).